Chapter 4

Corrosion Resistance and Electrocatalytic Properties of Metallic Glasses

Shanlin Wang

Additional information is available at the end of the chapter

http://dx.doi.org/10.5772/63677

Abstract

Metallic glasses exhibit excellent corrosion resistance and electrocatalytic properties, and present extensive potential applications as anticorrosion, antiwearing, and catalysis materials in many industries. The effects of minor alloying element, microstructure, and service environment on the corrosion resistance, pitting corrosion, and electrocatalytic efficiency of metallic glasses are reviewed. Some scarcities in corrosion behaviors, pitting mechanism, and eletrocatalytic reactive activity for hydrogen are discussed. It is hoped that the overview is beneficial for some researcher paying attention to metallic glasses.

Keywords: metallic glass, corrosion resistance, pitting corrosion, electrocatalytic property

1. Introduction

Except for high compression strength, microhardness, electrical resistivity, and good soft magnetic properties, most metallic glasses exhibit excellent corrosion resistance. The excellent corrosion resistances of metallic glasses are mainly attributed to the homogeneous single glass phase, the alloy chemistry, and the presence of metalloids [1–3]. No grain boundaries, dislocations, and other defects where corrosion can occur preferentially are expected to allow the growth of a uniform protective film. The chemical homogeneity is believed for rapid cooling rates required to produce full amorphous structure since no enough time is available for solid-state diffusion, that is, it is impossible for the formation of second phases, precipitation, and segregations. The homogeneity in chemical composition and microstructure promotes amorphous oxide formation on the surface which retards ionic transport. The

improvement of corrosion resistance is also considered to link to the ability of these metastable alloys to form supersaturated solid solution in one or more alloying elements. The alloying element available in solid solution may be incorporated into the oxide film to enhance its passivity. Thus, the effect of the amorphous structure, chemical and structural homogeneity, and the possibility of forming unique chemical composition not typical of near-equilibrium crystalline alloys are mostly considered as factors that can affect the corrosion properties of metallic glass.

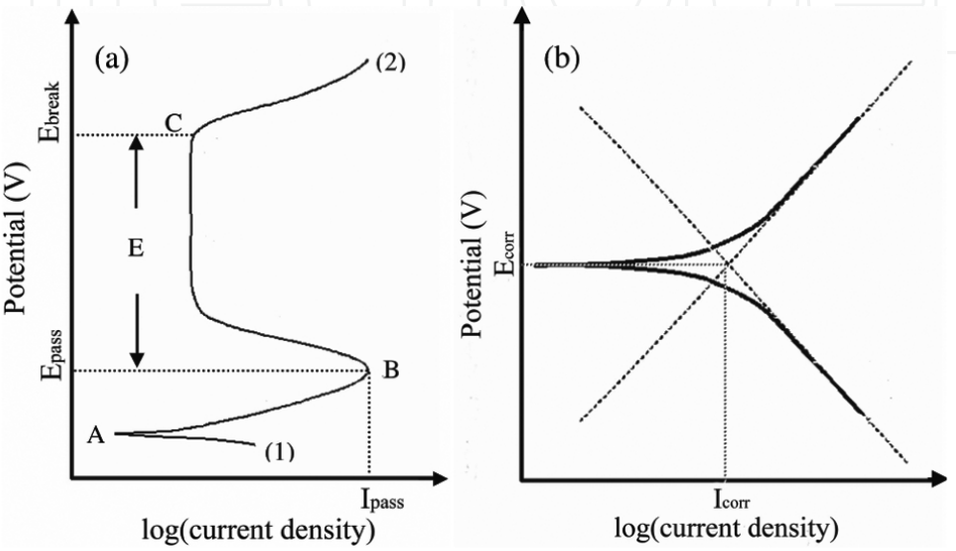

Figure 1. A schematic diagram of potentiodynamic polarization: (a) the theoretical anodic polarization curve, (b) the calculation of corrosion potential and corrosion current density.

In order to estimate the corrosion resistance, immersion test is one of method to calculate the average corrosion rate in one year, while the electronic chemistry methods such as the potentiodynamic polarization are applied in most researches, where the considerable information on the electrode processes can be attained, such as corrosion potential (E_{corr}), corrosion current density (I_{corr}), corrosion rate, pitting susceptibility, passivity, and the cathodic behavior. A schematic curve of the theoretical anodic polarization (a) and the calculation of corrosion potential and corrosion current density (b) are illustrated in **Figure 1**. As can be seen in **Figure 1(a)**, the scan start forms point (1) and progresses in the positive potential direction until termination at point (2), the open circuit potential is located at point A. At the potential, the sum of the anodic and cathodic reaction rates on the electrode surface is zero. As a result, the measured current will be closed to zero. With the increase of the potential, it moves to active region. In this region, metal oxidation is the dominant reaction taking place. Point B is known as the passivation potential, and as the applied potential increases above the value the current density is seen to decrease until a low, passive current density is achieved in passive region E. Once the potential reached a sufficiently positive value, that is located as point C, sometimes termed the breakaway potential, the applied current rapidly increases. Around the open circuit potential, a new line is fitted according to the linear regions of the polarization curve as illustrated in **Figure 1(b)**. The current density at that point is the corrosion current density

http://dx.doi.org/10.5772/63677

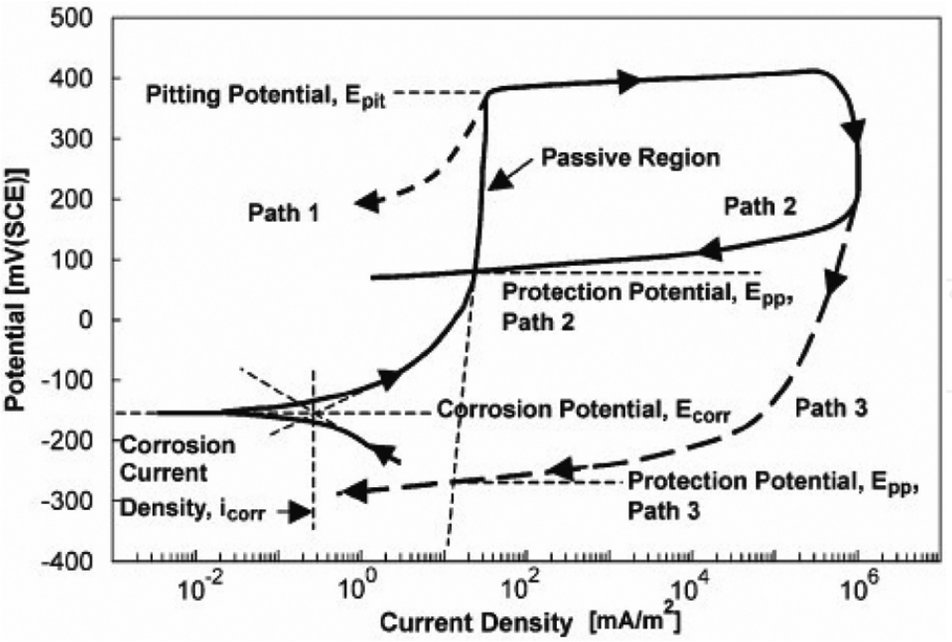

Figure 2. A schematic cyclic-anodic-polarization curve [4].

(I_{corr}) and the potential at which it falls is the corrosion potential (E_{corr}). It is generally agreed that the higher is the corrosion potential, the more difficult is the occurrence of the oxidation reaction for the metals, moreover, the larger is corrosion current density, the higher is corrosion rate, that is, the lower corrosion resistance for metallic glass.

While for the susceptibility of pitting corrosion, the cyclic-anodic-polarization is usually measured, and some parameters and typical characteristics with regard to pitting corrosion susceptibility are defined in the schematic polarization curves of **Figure 2** [4]. A potential scan is started below the corrosion potential, E_{corr}. At E_{corr}, the current density goes to zero, and then increases to a low and approximately constant anodic value in the passive range. In this range, a thin oxide/hydroxide film, a passive film, protects the material from high corrosion rates. If the current density decreases when the potential scan direction is reversed, as in path 1, the material is shown to be immune to pit corrosion. However, if on the potential up scan, the current density suddenly increases, and remains high on the down scan, until finally decreasing to the passive-region value, as in path 2, the material is shown to undergo a form of pitting corrosion. The potential at which the current density suddenly increases (pitting initiation) is known as the pit potential, E_{pit}, and the potential at which the current density returns to the passive value is known as the repassivation potential or the protection potential, E_{pp}. Between E_{pit} and E_{pp}, pits are initiating and propagating. In the case of path 2, pits will not initiate at E_{corr}, the natural corrosion potential; and, therefore, the material will not undergo pitting corrosion under natural corrosion conditions. If, on the other hand, path 3 is exhibited, where E_{pp} is below E_{corr}, the material will undergo pitting corrosion at surface flaws or after incubation time periods at E_{corr}. In terms of the overall resistance to pitting corrosion, two parameters of ($E_{pit} - E_{corr}$) and ($E_{pp} - E_{corr}$) are important. Higher values of both are desirable to reflect high values of E_{pit} and E_{pp} relative to E_{corr}.

2. Corrosion resistances of nonferrous metallic glasses

Metallic glass is comparatively newcomer to the amorphous material group, which is fabricated from a cooled liquid without crystallization under a rapid cooling rate. As the first metallic glass of $Au_{80}Si_{20}$ was discovered in 1960 by Duwez and coworkers [5], a series of metallic glasses such as Zr-, Ti-, Pd-, Cu-, Fe-, and Mg-based alloys are successfully fabricated by the method of melt quenching. In order to extend the industrial application of metallic glasses, the corrosion behaviors of metallic glass have been of great interest. The corrosion resistance of nonferrous metallic glass of Cu-, Ti-, Zr-, and Mg-based alloys will be discussed in the following part.

2.1. Effect of composition

Among of nonferrous metallic glasses, Zr-based metallic glass (Zr-MG) is investigated abroad in corrosion resistances. Addition of minor element such as Ag, Cu, Y, Ti, Ni, and Nb has been utilized to enhance the glass forming ability and resistance to general and local corrosion. Inoue and coworkers [6–10] have investigated the effect of Ni on the corrosion resistance of Zr-Ni-Cu-Al alloy. Zr-MG without Ni shows lowest corrosion potential and no obvious passivation region, but pitting directly can be observed as potential rises. Zr-MG with Ni is spontaneously passivated with current density around 10^{-3} A/m^2 before the occurrence of pitting corrosion in chloride solution. Since the Cu element in the Zr-MG is easily dissolved in chloride solutions, thus leads to a low corrosion resistance. The additional Ni inhibits the formation of soluble Cu-Cl films and facilitates forming the protective surface films with a high concentration of Zr cation, leading to a denser, thicker, and more pitting resistance ZrO_2 passive film. Zhang and coworkers [11, 12] reported that partial substitution of Ni and Co by Ag was effective in improving the corrosion resistance of Zr-MG, as the Ag addition increases the concentration of Zr and decreases the concentration of Al in the surface passive films, while Liu and coworkers [13] found that the addition of Ag could promote the formation of Al_2O_3 but slightly suppressed the formation of ZrO_2. The cast $Zr_{56}Al_{16}Co_{28-x}Nb_x$ (x = 1, 3, and 5 at%) metallic glass are spontaneously passivated in NaCl solution with a passive current density between 10^{-5} and 10^{-6} A/cm^2, and the pitting potentials shift to positive direction with the increasing of Nb content [14]. Though the Nb-bearing alloy's pitting potential and passive region are larger than Nb-free alloy, after pitting, however, the alloy with 4 at% Nb exhibits higher corrosion current density than Nb-free alloy, as shown in **Figure 3**, meaning that the corrosion reactions in Nb-bearing alloy are more severe at high potential [15]. Generally, the addition of Nb element in Zr-MG can facilitate the formation of highly protective Zr-, Al-, and Nb-enriched surface film, while Cu addition will deteriorate the passivation [16]. For $Zr_{55}Al_{10}Ni_5Cu_{30}$ metallic glass alloy, the mass loss and the average corrosion rate decrease with increase of Ti content in 1 M HCl solution [17], and the Ti addition improves the stability of passive film and pitting resistance, while they are susceptible to pitting corrosion [18].

Compared to Zr-MG, Cu-based metallic glasses with their superiority in price and mechanical properties possess great potential applications in the fields, such as bipolar plate materials, biomedical instruments, and microdevices. The investigations about corrosion resistance have

http://dx.doi.org/10.5772/63677

been carried extensively. Small addition of Nb, Cr, Ta, and Mo has proved to be effective in improving the corrosion resistance [19–21]. Asami et al. [19] investigated the effect of small addition of Nb, Mo, and Ta to $Cu_{60}Zr_{30}Ti_{10}$ at% metallic glass in 1 M HCl, HNO_3, NaOH, and 0.5 M NaCl solutions. The results demonstrate that Nb element is most effective in decreasing the corrosion rate in all of the solutions, moreover, the corrosion rate decreases with increasing the Nb content. The minor element addition can enhance the stability of passive film enriched in ZrO_2 and TiO_2. Except the minor addition Mentioned above, some rare metal element additions of In, Y, Ce, and Ln to Cu-MG are effective to improve the corrosion resistance [22–25]. The results demonstrate that the dissolution of rare element is favorable to forming continuous Zr-, Ti-rich protective oxide film and alleviates the local corrosion and propagation at the initial corrosion stage. The Ln addition can increase the nearest neighbor atomic distance affecting the topological instability, which is attributed to the improvement of corrosion resistance.

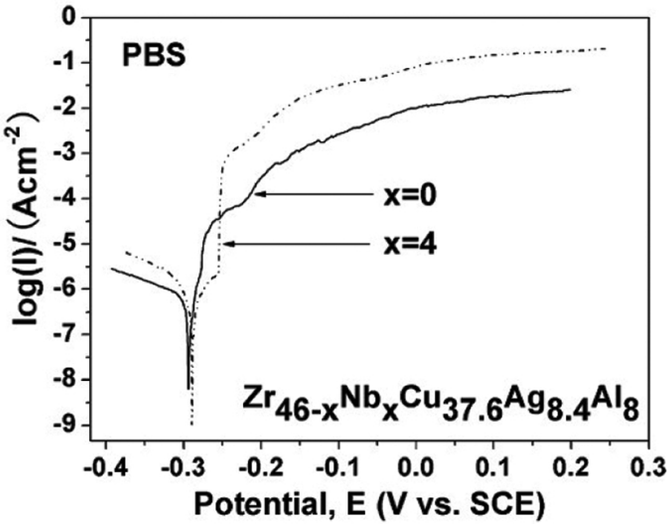

Figure 3. Potentiodynamic polarization curves for the alloy in phosphate-buffered solutions at 37°C [15].

As conventional titanium alloy, Ti-based metallic glass with high yield strength, low Young's modulus, high corrosion resistance can be applied as biomaterial [26], and mostly possesses higher corrosion resistance than Ti-6Al-4V alloy in a simulated body fluid environment. The minor element addition of Zr, Nb, and Cu will change the corrosion behavior of Ti-MG [27–29]. Nb addition can enhance the pitting resistance due to an improvement of the passive layer properties for near-homogenous alloys. Small addition of Zr promotes the corrosion potential and decreases the corrosion current density. The addition of Cu can shift the beginning of polarization reaction to a positive voltage level, while provokes severe Cu-induced selective dissolution under the higher applied voltage levels, resulting continuous pitting and the depletion of Ti and Zr in the alloy. With increase of (Ti + Zr)/Cu ratio, the pitting corrosion resistance is greatly enhanced due to the formation of surface film mainly composed of TiO_2 and ZrO_2.

As well known, magnesium alloy is also one of biomaterials. Recently, the corrosion behavior of Mg-based metallic glass is investigated. Wang et al. [30] reported that the Mn addition can promote the formation of a dense passive film, which delays the corrosion of the matrix. The Zn addition provokes the formation of $Zn(HO)_2$ and $Mg(OH)_2$, and the evolution of the corrosion process of the MgZnCa glass is schematically illustrated in **Figure 4** [31]. When Mg-MG is immersed in body fluid, the anodic dissolution of magnesium occurs and the magnesium hydroxide layer well is formed on the surface of the sample. The attack of Cl^- occurs at the weak sites of the magnesium hydroxide layer and transforms the magnesium hydroxide into soluble magnesium chloride. The fresh substrate, exposed to the medium directly, suffers further corrosion, and results in the releasing of Mg^{2+} and Zn^{2+}, as shown **Figure 4(a)**. As immersion prolonged, the Zn^{2+} concentration is increasing due to the continuous dissolution of Zn. The $Zn(OH)_2$ precipitates preferentially, compared to that of $Mg(OH)_2$ (**Figure 4(b)**), the $Zn(OH)_2$ precipitations will repair the defects in the surface layer, and then forms a continuous and uniform layer. With the corrosion proceeding, the corrosion product layer will be thickened and $Zn(OH)_2$ precipitation spreads, which are evidently depicted in **Figure 4(c)**. Meanwhile, the undissolved $Mg(OH)_2$ and $Zn(OH)_2$ precipitation can provide favorable sites for apatite nucleation. With Ti addition, the protective film of $Mg(OH)_2$ will enrich Ti, improving the stability [32].

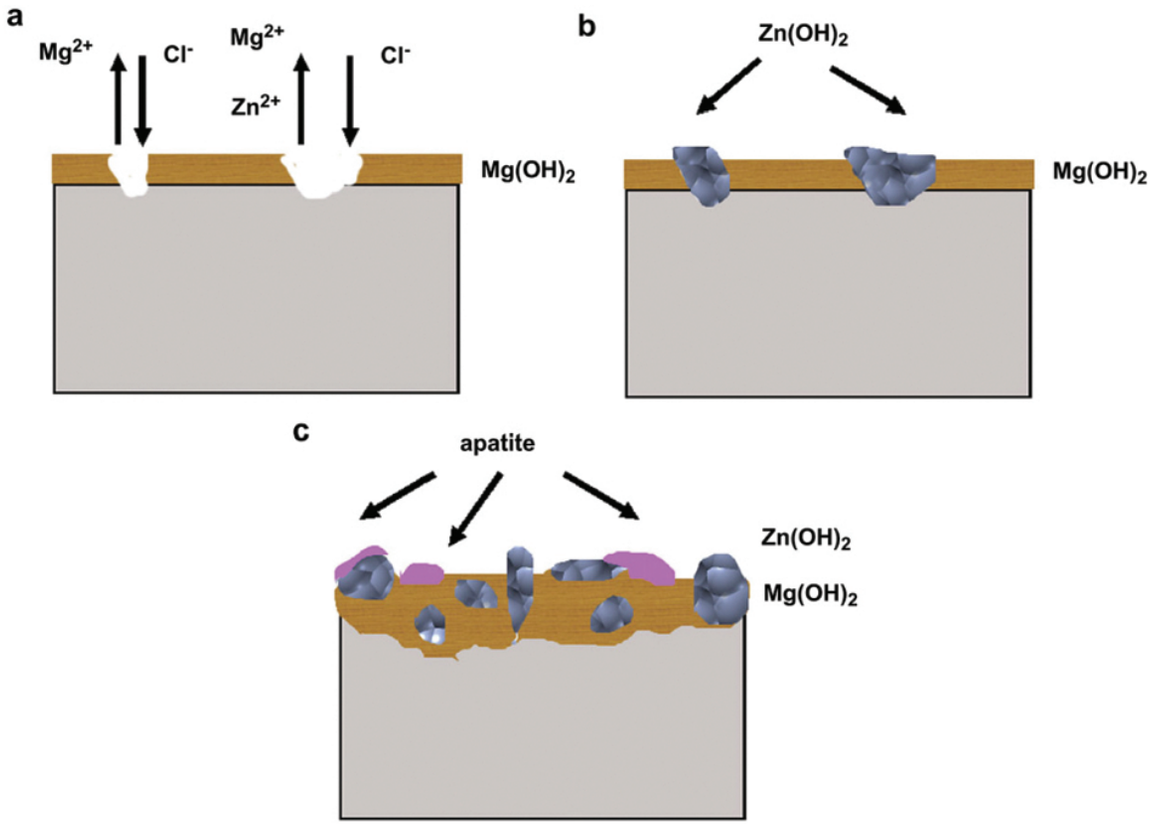

Figure 4. The sketch map for the evolution of corrosion process of Mg-Zn-Ca bulk metallic glass immersed in SBF: (a) initial stage, (b) middle stage, (c) final stage [31].

http://dx.doi.org/10.5772/63677

2.2. Effect of microstructure

The microstructure and composition homogeneities are destroyed with the crystallization, which is necessary to deteriorate the corrosion resistance of metallic glasses. $Zr_{56}Al_{16}Co_{28}$ metallic glass exhibits a decrease of passivation potential and an increasing of penetration rate with increasing heating temperature in Ringer's simulated body fluid at room temperature [33]. The corrosion parameters of some metallic glasses are summarized in the **Table 1** [34–39]. It can be attained that the corrosion resistance of most metallic glasses after crystallized will decrease, as shown that the corrosion potential decreases and the corrosion current density increases relatively, suggesting that the passive films formed on the surface of the glassy alloy in the anodic process are protective and denser than those on the crystal alloys. However, another metallic glasses exhibit more positive corrosion potential and low corrosion current density after crystallized, meaning that the crystalline alloy possesses excellent corrosion resistance, compared to metallic glass with same composition, since the nanocrystal phase such as a-Ti, CuZr precipitation or the reduction of the free volume in amorphous state that in turn reduces the average atomic distance.

Composition	State	E_{corr} (mV)	I_{corr} (A/cm²)	E_{pit} (mV)	E_{pit}–E_{corr} (mV)	I_{pass} (A/cm²)	CPR (um/y)	Temp (K)	Solution
$Zr_{62.3}Cu_{22.5}Fe_{4.9}Al_{6.8}Ag_{3.5}$ [34]	Am.	−290	5.5×10^{-8}	−22	268	---	1.5	310	PBS
	Cry.	−305	7.7×10^{-8}	−45	160	---	0.9	310	PBS
$Ti_{40}Zr_{10}Cu_{38}Pd_{12}$ [35]	Am.	−31	4.6×10^{-7}	---	---	---	---	---	HBSS
	Cry.	−61	2.0×10^{-8}	---	---	---	---	---	HBSS
$Ti_{42}Zr_{40}Si_{15}Ta_3$ [36]	Am.	−455	4.9×10^{-8}	113	---	2.9×10^{-6}	---	310	SBF
	Cry.	−321	8.7×10^{-8}	176	---	4.0×10^{-6}	---	310	SBF
$Zr_{60}Cu_{20}Al_{10}Fe_5Ti_5$ [37]	Am.	−214	3.0×10^{-4}	---	---	---	---	310	SBF
	Relx	−43	8.8×10^{-6}	39	83	---	---	310	SBF
	Cry.	−22	1.4×10^{-6}	407	429	---	---	310	SBF
Zr_2Ni [38]	Am.	−354	1.3×10^{-7}	82	---	1.1×10^{-6}	---	300	0.1 M NaCl
	Cry.	−369	1.4×10^{-7}	76	---	9.3×10^{-7}	---	300	0.1 M NaCl
$Cu_{47.5}Zr_{47.5}Al_5$ [39]	Am.	−760	1.2×10^{-7}	110	870	5.2×10^{-7}	---	300	ASS
	Cry.	−460	5.0×10^{-8}	110	570	1.6×19^{-6}	---	300	ASS

Table 1. Summary of corrosion parameters for some metallic glasses and its crystalline alloys from literature reports.

Wang et al. [40, 41] reported that the corrosion resistance of Mg-MGs was slightly reduced when the in situ second phase or reinforcement phase were induced into metallic glass. It is believed, when corrosion is developing, the continuous distribution of glass matrix might be able to prevent corrosion from spreading from one a grain to another a grain directly across

the glass matrix. Then corrosion is stopped after the crystalline phases dissolves and a continuous glass matrix is exposed to solution. If the crystalline phase is nanoparticle and presents high chemical potential, the corrosion resistance of metallic glass composite will not reduce, even increase for some metallic glass alloy [39, 42].

When bulk metallic glass is fabricated into metallic glass coating, the corrosion resistance of metallic glass coating is affected not only by the composition, but also by the surface and porosity of the metallic glass coating [43]. The effect of porosity on corrosion resistance for Ti-MG evaluated with potentiodynamic polarization is shown in **Figure 5** [44]. The metastable current transition of different magnitude can be observed for the porous bulk metallic glass. Although rapid increase in anodic current due to pitting is not observed, anodic current density slightly increases, indicating that some of metastable pitting occur within the pore at the same time and afterward are stabilized by the pore wall during the anodic polarization process. Undoubtedly, the existing of pores would result in crevice corrosion, where potentiodynamic polarization curve exhibits a slow increase of current density in the anodic polarization part. Gebert et al. [45] reported that the state of surface finishing of Zr-based metallic glass remarkably influences its corrosion and passivity. It is considered that the smoothness, homogeneity, and the modification of surface chemistry such as Cu concentration on the surface of Zr-MG are modified after polished with different polishing materials.

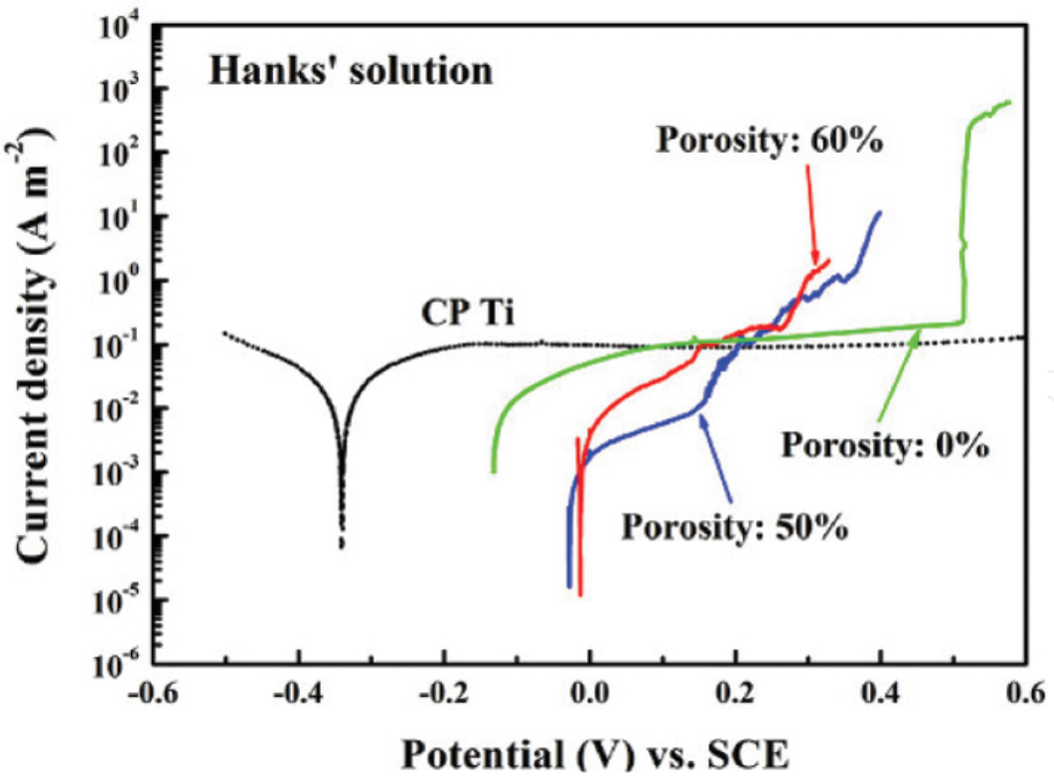

Figure 5. Potentiodynamic polarization curves of the produced porous $Ti_{45}Zr_{10}Cu_{31}Pd_{10}Sn_4$ bulk metallic glass with various porosities in Hanks' solution at 310 K compared to pure Ti alloy [44].

http://dx.doi.org/10.5772/63677

Besides chemical and physical defects of glassy alloy, the mechanically generated defects can enhance the corrosion susceptibility. Gebert et al. [46] reported that a slight improvement of spontaneous passivity but a decrease of resistance against chloride-induce pitting were detected when Zr-based bulk metallic glass was shot-peened with long time, and the corrosion damage evolution was governed by the nature of the mechanically generated defects, such as craters, cracks of scratches and their surrounding stress fields. The effect of shear bands breaking through a sample surface on corrosion processes in acidic environments is investigated. The preferential sites for corrosion initiation and propagation are formed along the shear bands, as shown **Figure 6** [47]. The local chemical and structural changes in the close vicinity of the shear band zone are mainly predisposing factor. An et al. [48] found that the Cu-MG after tensioned exhibited more negative corrosion potential and larger corrosion current density in chloride solution, which indicated the deterioration of corrosion resistance of Cu-MG tensioned, compared with as-cast.

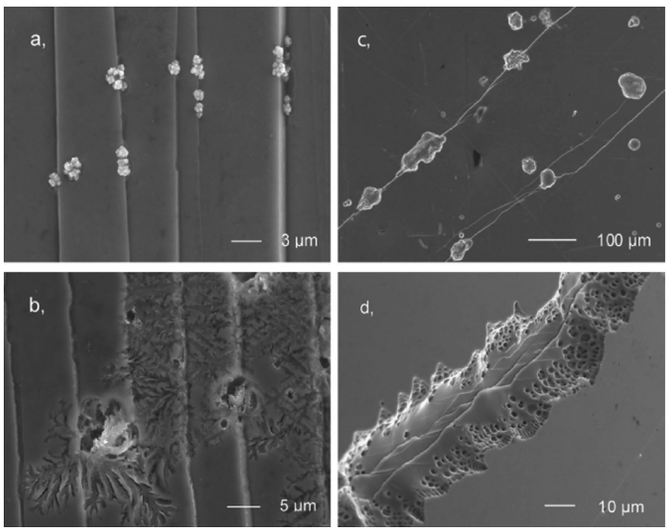

Figure 6. SEM images of corroded shear band regions at surfaces of predeformed Zr-based metallic glass after exposure to 12 M HCl: (a, b) bent ribbon; (c, d) lateral area [47].

2.3. Effect of environment

Though the microstructure and chemical composition of nonferrous affect the corrosion resistance, it is evident from **Table 2** that the environment is also a significant factor in the corrosion properties. **Table 2** provides corrosion parameters for some nonferrous metallic glass in various electrolytes. Pourgashti et al. [49] found that Zr-MG exhibited excellent corrosion resistance in 3.5% NaCl solution, and showed better corrosion resistance than 316L in HNO_3 and H_2SO_4 solutions. It can be seen from **Table 2** that the tendency of corrosion current density I_{corr} is $I_{corr/HCl} > I_{corr/HNO3} > I_{corr/NaCl} > I_{corr/H2SO4}$. The Zr-MG reveals to increase in passive current density and decrease of transpassive potential with increase in nitric acidic concentration [51]. Gebert et al. [50, 55] reported that $Zr_{55}Cu_{30}Al_{10}Ni_5$ was immune to localized corrosion in alkaline solution. However, a susceptibility to pitting corrosion was observed

during anodic polarization experiment at chloride concentration as low as 10^{-3} M. Moreover, the effect of temperature on the corrosion resistance was investigated. The Zr-MG exhibits that E_{pit} decreases as the temperature increases, indicating an increased tendency of pitting in the chloride solutions as the temperature is increasing.

Composition	E_{corr} (mV)	I_{corr} (A/cm^2)	E_{pit} (mV)	$E_{pit}-E_{corr}$ (mV)	I_{pass} (A/cm^2)	CPR (um/y)	Temp (K)	Solution
$Zr_{41.2}Ti_{13.8}Ni_{10}Cu_{12.5}Be_{22.5}$ [49]	−469	6.7×10^{-7}	97	---	---	10	298	3.5% NaCl
	−428	9.0×10^{-7}	---	---	---	80	298	1 M HNO_3
	−491	5.4×10^{-7}	---	---	---	620	298	0.5M H_1SO_4
	−322	1.4×10^{-6}	---	---	---	260	298	1 M HCl
$Zr_{55}Cu_{30}Al_{10}Ni_5$ [50]	---	---	450	---	---	---	298	0.001 M NaCl
	---	---	50	---	---	---	423	0.001 M NaCl
	---	---	−100	---	---	---	523	0.001 M NaCl
$Zr_{59}Ti_3Cu_{20}Al_{10}Ni_8$ [51]	603	2.3×10^{-8}	1450	---	1.1×10^{-7}	---	298	1 M HNO_3
	357	5.6×10^{-7}	1370	---	2.2×10^{-6}	---	298	6M HNO_3
	818	3.4×10^{-6}	1200	---	9.8×10^{-5}	---	298	11.5M HNO_3
$Cu_{55}Zr_{35}T_{10}$ [52]	18.9	2.4×10^{-4}	---	---	---	33.2	298	0.005M HCl
	−10.2	1.2×10^{-4}	---	---	---	82.5	298	0.01 M HCl
	−119.6	2.0×10^{-4}	---	---	---	342	298	0.5M HCl
	−322.9	1.2×10^{-3}	---	---	---	702	298	1 M HCl
	164.9	2.7×10^{-5}	---	---	---	2.6	298	0.005M NaCl
	−21.1	2.3×10^{-5}	---	---	---	7.7	298	0.01 M NaCl
	−58.0	1.8×10^{-4}	---	---	---	37.6	298	0.5M NaCl
	−87.6	6.4×10^{-5}	---	---	---	79.2	298	1 M NaCl
$Ti_{46}Cu_{27.5}Zr_{11.5}Co_7Sn_3Si_1Ag_4$ [53]	−270.8	2.7×10^{-4}	---	---	---	---	310	PBS
	−151.7	2.0×10^{-4}	---	---	---	---	298	0.9 wt% NaCl
	−289.8	1.6×10^{-4}	---	---	---	---	298	1 M HCl
	−345.6	1.4×10^{-3}	---	---	---	---	298	1 M NaOH
$Mg_{69}Zn_{27}Ca_4$ [54]	−1120	---	−976	144	---	---	320	SBF
	−1330	---	87	1417	---	---	320	PBS

Table 2. Summary of corrosion parameters for some metallic glasses in different corrosive environment.

http://dx.doi.org/10.5772/63677

As similar to Zr-MG, $Cu_{60}Zr_{20}T_{20}$ metallic glass during the potentiodynamic polarization exhibits the active dissolution state in the whole anodic region in different solutions [56]. The current density increases to a very high value after the E_{corr} is reached indicating high rate of metal dissolution and no sign of passivity is observed. The higher the concentration of chloride, the higher is the I_{corr} value which in turn indicates that the rate of corrosion increases with increase in concentration of Cl^-. The E_{corr} becomes more negative with the increase in concentration of solution. The tendency of I_{corr} and E_{corr} also can be seen in **Table 2** for Cu-, Ti- and Mg-based metallic glass.

3. Corrosion resistance of Fe-based metallic glass

Due to its high strength, good soft magnetic properties, excellent corrosion resistance, and low producing cost, Fe-based metallic glass is attended extensively to the researchers in material science and technology fields around the world. Besides the glass forming ability, strength, and soft magnetic properties, the investigation on corrosion resistance is interesting for the industrial application of Fe-based metallic glasses.

3.1. Enhance of minor element addition

The effects of the addition of a small amount of metallic elements such as Cr, Mo, Nb, W, Ni, Ta, Y, Al, Co, and Mn on the corrosion resistance of Fe-MGs are investigated by means of electrochemical polarization and weight loss measurements. It is well known that chromium is an effective element enhancing corrosion resistance of Fe-MGs. In Fe-Co-B-Si-Nb metallic glass [57], the corrosion rate decreases from 0.7 mm/year for Cr-free alloy to 6×10^{-2} mm/year for the alloy with 4 at% Cr in 0.5 M NaCl solution at 298 K. For the $Fe_{73.5}Si_{13.5}B_9Nb_3Cu_1$ metallic glass in marine environments, the corrosion rate is 14 times lower for the material with 2 at% Cr and 88 times lower for the material with 4 and 6 at% Cr as compared with the material in amorphous state without Cr [58]. Though increasing Cr concentration up to 8 at% Cr tends to stabilize the passive layer, the corrosion rate remains very high. The addition of 8 at% is not sufficient to the formation of a stable passive layer, and the materials are dissolved or undergo severe attack in 1, 2, and 5 M H_2SO_4 [59]. In 9.7 M H_2SO_4 solution at 70°C, the $Fe_{63.1}C_{7.1}Si_{4.4}B_{6.5}P_{8.6}Cr_{8.3}Al_{2.0}$ metallic glass exhibits high corrosion rate of 13 mm/year that is five times lower than that of AISI304L [60]. The crack width on the corrosion product layer after potentiostatic polarization measurement decreases with increase of content as shown in **Figure 7(a)** and **(b)**, the pitting morphology occurs on the surface of metallic glass with 6.3 at% Cr, as showed in **Figure 7(c)**, however, a homogenous surface without cracks or pitting is formed for the alloys with Cr content exceeding 8.3 at% as shown in **Figure 7(d)** and **(e)**, due to the formation of Cr-enrich passive film on the surface.

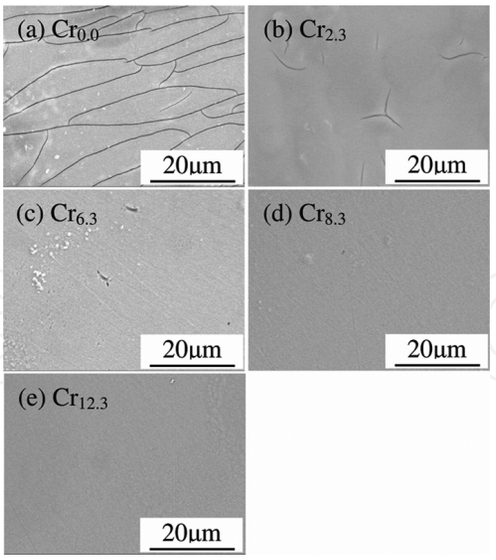

Figure 7. SEM micrographs on the surfaces in 9.7 M H_2SO_4 solution at 343 K: (a) x = 0.0, (b) x = 2.3, (c) x = 6.3, (d) x = 8.3, (e) x = 12.3 [60].

With minor addition of Y, not only glass forming ability, but also corrosion resistance is increasing evidently. The dependence of the electrochemical parameters upon the yttrium content is shown in **Figure 8** [61]. The corrosion current density I_{corr}, passive current density I_{pass}, corrosion potential E_{corr} from the polarization behavior and open-circuit potentials OCP of FeCrMoCBY metallic glass after immersion in 1 M HCl solution for 100 h as a function of Y content are presented, respectively. It can be seen that the passive current density is sensitive to the yttrium content. The effects of some metal element additions are summarized in **Table 3**. It is obvious that minor element addition into Fe-MG will evidently increase the corrosion resistance. The corrosion rate of FeBSiNb alloy with 0.4 at% Ni addition is about 1000 times lower than that without Ni addition in 0.5 M NaCl [62]. Generally, the minor element additions such as Mo, Y will provoke the formation of passive film, resulting in improvement of corrosion resistance [61, 65].

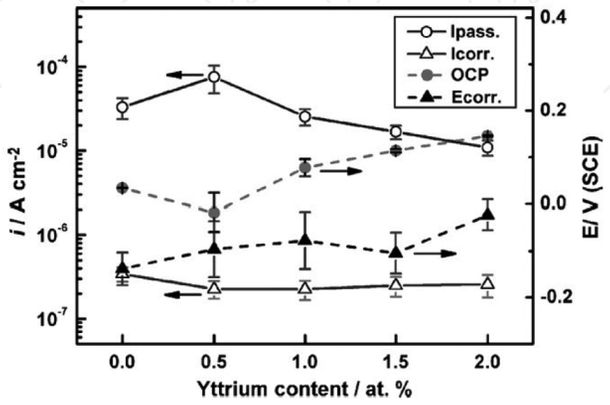

Figure 8. The statistical analysis of the various electrochemical parameters obtained from polarization behavior of immersion tests of Fe-MG with the variation of yttrium content [61].

Composition	Elem. X	Content (at%)	E_{corr} (mV)	I_{corr} (A/cm^2)	E_{pit} (mV)	I_{pass} (A/cm^2)	CPR (um/y)	Temp (K)	Solution
FeBSiNbX [62]	Ni	0	−626	4.5×10^{-6}	---	---	897	298	0.5M NaCl
		0.2	−426	3.2×10^{-7}	---	7.9×10^{-6}	1.8		
		0.4	−367	1.2×10^{-7}	---	4.1×10^{-6}	< 1		
		0	−936	5.9×10^{-6}	---	---	978		0.5M NaOH
		0.2	−677	9.9×10^{-7}	---	1.6×10^{-5}	56		
		0.4	−647	7.0×10^{-7}	---	1.1×10^{-5}	32		
		0	−404	7.0×10^{-5}	---	9.3×10^{-3}	2106		0.5M H_2SO_4
		0.2	−356	3.4×10^{-6}	---	1.9×10^{-3}	787		
		0.4	−334	1.1×10^{-6}	---	1.0×10^{-3}	674		
FeBCuX [63]	Nb, Zr	3.5, 3.5	---	---	−170	---	---	298	NaCl+NaOH (pH13)
	Nb, Mo	3.5, 3.5	---	---	−270	---	---		
	Zr. Mo	3.5, 3.5	---	---	−310	---	---		
	Mo	7	---	---	−340	---	---		
FeCrMoBCX [64]	Nb	0	−169	---	715	2.5×10^{-6}	---	310	RS(pH6)
		3	−45	---	876	2.0×10^{-7}	---		
		4	122	---	1299	3.8×10^{-8}	---		
FeBCrX [65]	Mo, Nb	0	---	---	---	$2.8 \times 10^{-3*}$	---	289	0.1 M H_2SO_4
	Mo,Nb	0.3, 0	---	---	---	$1.4 \times 10^{-3*}$	---		
	Mo,Nb	0, 0.3	---	---	---	$1.0 \times 10^{-3*}$	---		
	Mp,Nb	0.15, 0.15	---	---	---	$4.5 \times 10^{-4*}$	---		
FeCSiBPAlMoCoX [66]	Cr	0	−304	6.5×10^{-6}	---	1.2×10^{-2}	---	298	0.5M H_2SO_4
		2.3	−279	2.3×10^{-6}	---	1.9×10^{-4}	---		
		12.3	−235	7.0×10^{-7}	---	2.9×10^{-5}	---		
		0	−311	4.5×10^{-6}	---	7.9×10^{-3}	---		1 M HCl
		2.3	290	1.9×10^{-6}	---	2.8×10^{-4}	---		
		12.3	220	8.0×10^{-7}	---	1.7×10^{-5}	---		
FeCrNiX [67]	Si	20	−200	1.9×10^{-6}	---	---	---	298	0.01 M HCl
	P	20	−800	1.5×10^{-7}	---	---	---		
FeCrMoCX [68]	B	4	---	---	---	---	5~30	298	1 M HCl
		6	---	---	---	---	6–40		6M HCl
		8	---	---	---	---	25–70		12M HCl

Table 3. Summary of corrosion parameters affected by element addition for some metallic glasses.

Besides the metal elements, the metalloids element addition of B, Si, P, S, Ni, and C are also important to the corrosion resistance. The $Fe_{50-x}Cr_{16}Mo_{16}C_{18}B_x$($x$ = 4, 6, 8 at%) glassy alloys exhibits spontaneously passivation in 1 and 6 M HCl solutions with wide passive region and low passive current density [68]. With increase of boron content in alloys, the corrosion resistance of glassy alloys is improved, even in 12 HCl solution, the glassy alloy with 8 at% B do not suffer pitting corrosion. With P addition in the $Fe_{45}C_{16}Mo_{16}C_{15}B_{10}$ glassy alloy, the kinetics of passivation and composition of passive film are improved in HCl solution. While with Si replacement of P, the corrosion resistance can be enhanced due to the formation of passive film composed of chromium oxide with some amounts of silica [67].

3.2. Effects of microstructure homogeneity

Since metallic glasses are metastable and can be transformed into stable crystalline phase by heat treatment or mechanical working, the structural change can also affect corrosion resistance for metallic glasses. A comparison of passive current density I_{pass}, corrosion/transpassivation potential E_{corr} and corrosion rate CPR for some Fe-based metallic glasses and their crystalline alloy is summarized in **Table 4** [69–71]. It can be observed from **Table 4** that the corrosion/passive current density and corrosion rate increase for the crystalline alloys compared with metallic glass, while corrosion/transpassivation potential depends on their compositions.

Composition	State	E_{corr} (mV)	I_{pass} (A/cm^2)	CPR (um/y)	Temp (K)	Solution
FeCrMoCBY [69]	Amor	77	3.0×10^{-5}	---	298	1 M HCl
		200	6.0×10^{-5}	---		6M HCl
	Cryst	29	1.0×10^{-4}	---		1 M HCl
		152	---	---		6M HCl
FeSiB [70]	Amor	−735	---	---	298	0.5M NaCl
	Cryst	−765	---	---		
FeSiBNbCu [70]	Amor	−605	---	120	298	0.5M NaCl
	Cryst	−515	---	310		
FeZrB [71]	Amor	−520*	1.9×10^{-3}	---	298	0.5M H_2O_4
	Cryst	−463*	2.2×10^{-2}	---		
FeNbZrBCu [71]	Amor	−860*	1.0×10^{-3}	---	298	0.5M H_2O_4
	Cryst	−685*	1.3×10^{-2}	---		
FeNbB [71]	Amor	−1070*	7.5×10^{-4}	---	298	0.5M H_2O_4
	Cryst	−850*	1.0×10^{-2}	---		

Table 4. Summary of corrosion parameters affected by microstructure for some Fe-MGs.

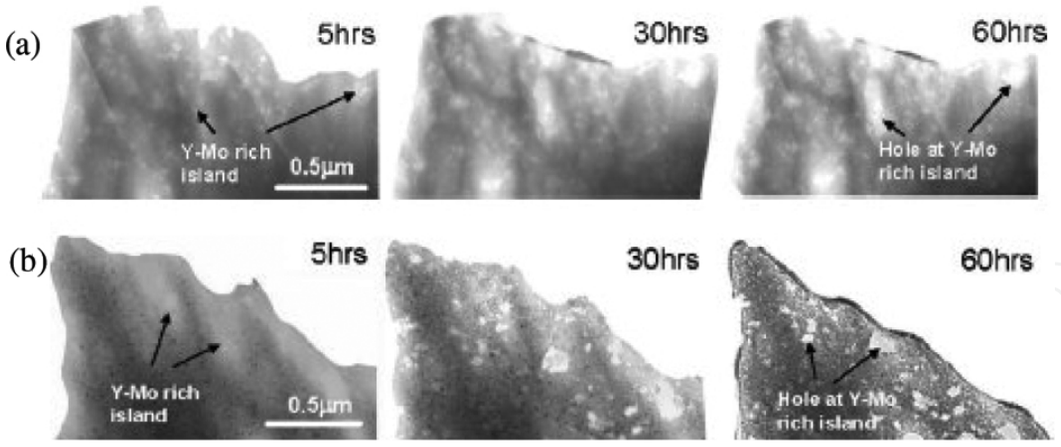

Figure 9. BF-TEM micrographs of (a) fully amorphous, (b) devitrified SAM 1651 after immersion in 6 M HCl for different periods of time [69].

The decrease of corrosion resistance in crystalline alloys obtained by the isothermal heat treatment of Fe-M-B (M = Nb, Zr) metallic glasses is explained by the formation of the α-Fe crystalline phase that has greater corrosion susceptibility in compared to that of the amorphous phase [70]. Long et al. thought the galvanic effects between adjacent phases with different composition were resulted in the deterioration of corrosion resistance for Fe-Co-B-Si-Nb metallic glass [72]. A comparison of BF-TEM morphologies for amorphous and devitrified SAM 1651 [69] is shown in **Figure 9**. It indicates that the lacier morphologies for devitrified SAM 1651 mean the degradation in the corrosion resistance. However, the abrupt increase in the corrosion potential for crystalline alloy is attributed to the decrease of the residual stress during densification, and the surface atom electrochemically active site [73]. Since atom at a glassy metal surface are in nonequilibrium configuration and may effectively sit on higher energy wells than that corresponding to atoms on an equilibrium configuration. Moreover, the faster migration of silicon ions to the surface in the crystalline structure promotes the SiO_2 film formation, which enhances the corrosion properties [74].

During the fabrication processing of bulk metallic glass and metallic glass coating, the porosity is not avoided due to rapid cooling. The effect of porosity on the corrosion resistance is investigated in some literatures [75–77].The corrosion resistance of coating 1 with the porosity of 0.04% is better than that of another two coatings with the porosity of 0.2% and 0.5%, respectively [75]. When the porosity decreases form 1.89% of low deposition rate to 1.22% of high deposition rate, the corrosion resistance of FeCrMoCBY amorphous coating increases evidently due to the elimination of through pores [76]. However, when the porosity is lower than 1.22%, the corrosion resistance seems more sensitive to the amorphous phase content. If the thickness of the coating decreases, the number of through-porosity in coating increases, which affects the corrosion resistance, as shown in **Figure 10** [77]. It indicates that through-porosity is much more detrimental to the corrosion resistance of the coated material compared with nonthrough porosity.

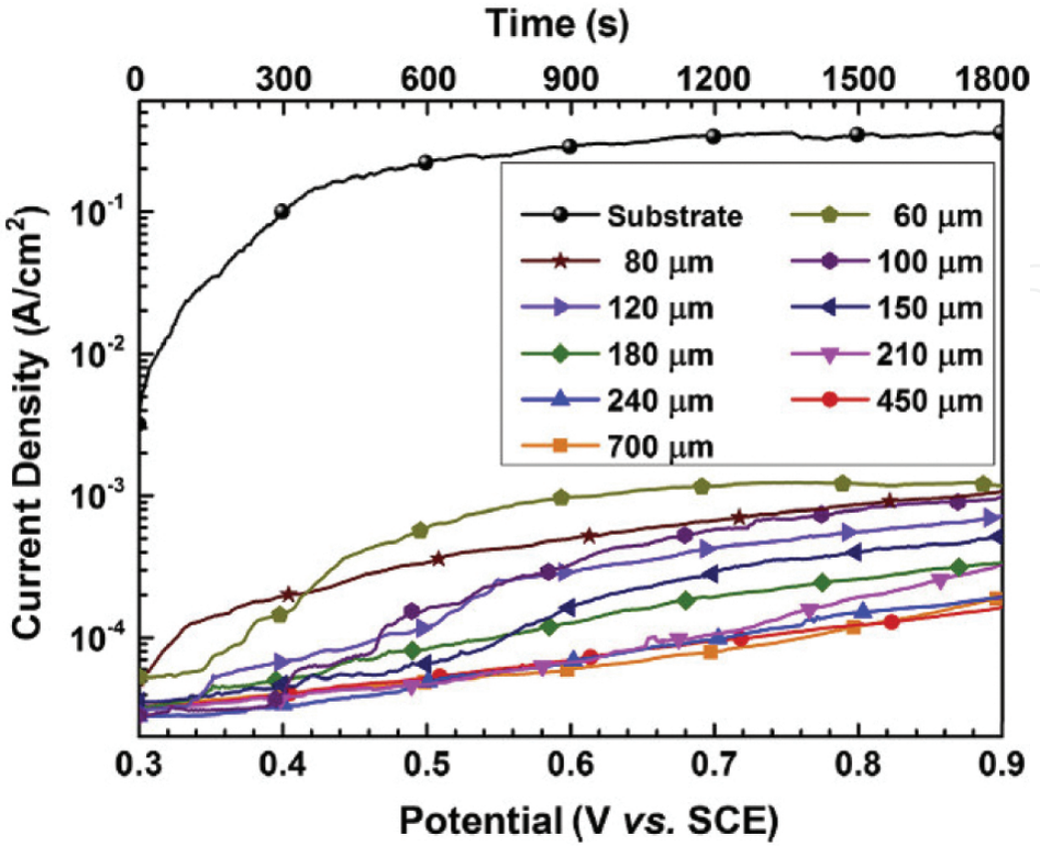

Figure 10. Anodic polarization conducted on the bare substrate and coated substrate with various thickness of Fe-MG coating in 3.5 wt% NaCl solution [77].

In some bulk metallic glass or metallic glass coating, the crystallize particles such as WC, TiN, SUS316, NbC, TiO_2, and Al_2O_3 are induced [78–83]. It is obvious that the crystallized particles are deteriorated the structural homogeneity. However, little investigations are done about the influence of crystalline particle on the corrosion resistance, which is important for the potential application of Fe-based metallic glass as anticorrosion and antiwearing materials.

3.3. Effects of service environment

The corrosion behaviors of Fe-based metallic glasses are affected by environmental factors. Intuitively, the stronger the aggressiveness of the solution is, the weaker the corrosion resistance of metallic glass exhibits. The results [68] attained in immersion experiments for $Fe_{48}Cr_{16}Mo_{16}C_8B_4$ glassy alloy in 1, 6, and 12 M HCl solutions exhibit, as expected, that the corrosion rate increases as the increase in concentration of HCl solution. The alloy occurs pitting on the surface after 168 h of immersion in the 12 M HCl solution at room temperature. FeCrMoCBP alloy is spontaneously passivated with a passive current density of about 10^{-1} A/m^2 and a wide passive region in 1 M HCl solution, however, its passive film is not stable by anodic polarization, as an anodic current density increases with increasing potential in 6 M HCl solution, and no passive film seems formed on the surface with rapid increasing of current

http://dx.doi.org/10.5772/63677

density in 12 M HCl solution [84]. $Fe_{54.2}Cr_{18.3}Mo_{13.7}Mn_{2.0}W_{6.0}B_{3.3}C_{1.1}Si_{1.4}$ (wt%) alloy can passivate spontaneously in the H_2SO_4 solution, and the passive current density is changed from 1×10^{-5} A/cm^2 with 0.4 M to 2×10^{-5} A/cm^2 with 0.1 M [85]. The corrosion penetration rates of $Fe_{48}Cr_{15}Mo_{14}Er_2C_{15}B_6$ metallic glass [86] are 39.9, 27.5, and 3 mm/year in 1 M HCl, 1 M NaOH, and 0.6 M NaCl with pH 7 solutions, respectively. The critical passivation potential E_{corr} and critical passivation current density I_{corr} of Fe-Ni metallic glass decrease with increase of pH value of solution, as shown in **Figure 11** [87].

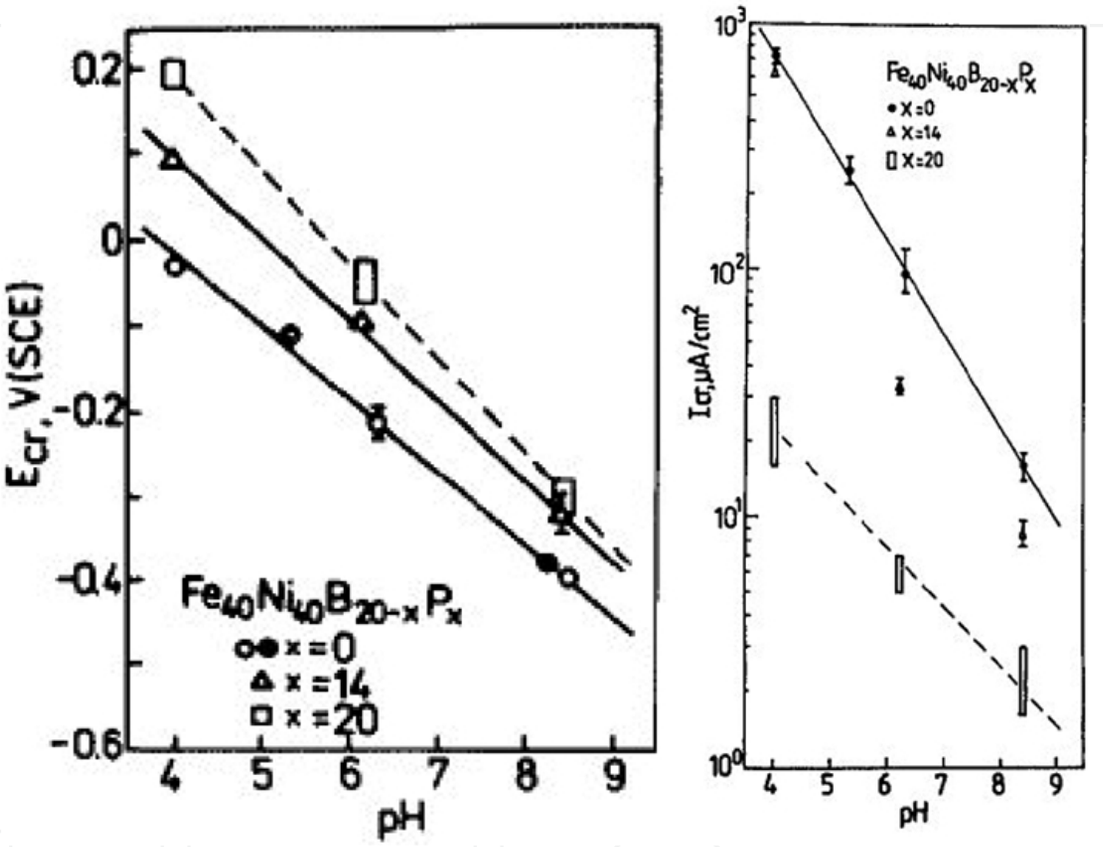

Figure 11. The effect on critical passivation potential E_{cr} and current density I_{cr} of Fe-Ni amorphous alloy at 298 K [87].

The corrosion rate of FeNiB metallic glass is only 70 μm/year in 3.5 wt% NaCl solution [73], while the corrosion rate increases to 130,000 μm/year in 1 M HNO_3 solution, near two thousand times larger than that in sodium chloride solution, as shown in **Table 5**. In **Table 5**, it is attained that more negative corrosion potential is obtained with increase of pH value, and the corrosion current density decreases. As the acidic ion or hydroxyl ion concentration increase, the corrosion potential becomes more negative and the corrosion current density increases generally. That is, the corrosion resistance decreases with increase of acidic ion concentration and hydroxyl ion content. When the concentration of hydrogen ion is same, the existence of chloride ion will deteriorate the corrosion resistance. In a word, the corrosion resistance of Fe-based metallic glass decreases as the solution aggressiveness increases.

Composition	E_{corr} (mV)	I_{corr} (A/cm^2)	E_{pit} (mV)	I_{pass} (A/cm^2)	CPR (um/y)	Temp (K)	Solution
FeNiB [88]	---	1.5×10^{-2}	---	---	130,000	298	1 M HNO_3
	---	1.5×10^{-3}	---	---	14,900	---	1 M NaOH
	---	8.0×10^{-5}	---	---	70	---	3.5 wt% NaCl
	---	1.3×10^{-4}	---	---	1140	---	1 M HCl
FeNiBAiNb [62]	−367	1.2×10^{-7}	---	1.1×10^{-6}	<1	298	0.5 M NaCl
	−647	7.0×10^{-7}	---	1.1×10^{-5}	32	298	0.5 M NaOH
	−334	1.1×10^{-6}	---	1.0×10^{-3}	674	298	0.5 M H_2SO_4
FeCSiBPCrAlMo [89]	−264	9.0×10^{-7}	---	---	---	298	0.5 M H_2SO_5
	−283	4.1×10^{-6}	---	---	---	298	1 M HCl
FeCoCrMoCBY [90]	−269	2.4×10^{-7}	1090	---	---	298	Hank's
	−315	4.8×10^{-8}	1200	---	---	298	Saliva
FeCrMoCBY [91]	−614	2.0×10^{-6}	988	$1.3 \times 10_{-3}$	---	298	3.5wt% NaCl
	−414	1.1×10^{-5}	904	1.7×10^{-3}	---	298	1 M HCl
	−377	4.6×10^{-6}	879	5.5×10^{-4}	---	298	1 M H_2SO_4
FeCoCrMoCBY [92]	---	---	---	---	0.12	298	1 M HCl
	---	---	---	---	0.12	298	1 M HNO_3
	---	---	---	---	0.13	298	1 M NaOH
	---	---	---	---	0.07	298	3.5 wt% NaCl
FeCrMnMoWBCSi [85]	−367	---	---	---	---	298	0.25 M H_2SO_4
	−219	---	---	---	---	298	0.25 M Na_2SO_4
	−455	---	---	---	---	298	0.5 M HCl
	49	---	---	---	---	298	0.5 M NaCl
FeCoCrMoCBY [93]	−257	4.7×10^{-8}	715	---	---	298	Acid rain
	−378	7.5×10^{-8}	1033	---	---	298	3.5 wt% NaCl
FeBNb [94]	−458	1.5×10^{-5}	---	---	---	298	NaCl+H_2SO_4pH1.0
	−700	1.5×10^{-5}	---	---	---	298	NaCl pH5.5
	−637	7.0×10^{-6}	---	---	---	298	NaCl+NaOH pH10
FeCoBSiNb [94]	−381	1.5×10^{-5}	---	---	---	298	NaCl+H_2SO_4 pH1.0
	−550	2.0×10^{-6}	---	---	---	298	NaCl pH5.5
	−509	1.5×10^{-6}	---	---	---	298	NaCl+NaOH pH10
FeCrNiB [94]	−192	6.0×10^{-8}	---	---	---	298	NaCl+H_2SO_4 pH1.0
	−128	1.5×10^{-8}	---	---	---	298	NaCl pH5.5
	−209	2.0×10^{-8}	---	---	---	298	NaCl +NaOH pH10

Table 5. Summary of corrosion parameters affected by environment for some Fe-MGs.

http://dx.doi.org/10.5772/63677

4. Pitting corrosion of metallic glasses

Though metallic glass exhibits excellent general corrosion resistance, it is also susceptible to pitting corrosion in aggressive solutions, especially containing Cl^- ion [95]. Since the surface film is not stable during the anodic polarization, many pits are observed on the surface of FeCrMoCB metallic glass with 4 at% B immersed in 12 M HCl solution for 168 h [68]. During potentiodynamic polarization in 1.7 M HCl solution, many peaks of current density occur for FeCrMB (M = Mo, Nb) metallic glass, which is attributed from pitting corrosion. Moreover, the morphologies of pits are confirmed by SEM analysis after the immersion test [65]. $Fe_{52}Mn_{10}Mo_{14}Cr_4B_6C_{14}$ metallic glass is susceptible to pitting corrosion, although presents good corrosion resistance characterized by a low passivating current in 0.6 M NaCl solution [96]. $Fe_{48}Cr_{15}Mo_{14}B_6C_{15}Y_2$ metallic glass, as known SAM1651, exhibits hysteresis loop during cyclic potentiodynamic polarization in 4 M NaCl solution at 373 K, which indicates the formation of localized corrosion [97]. Pardo et al. [58, 59] found that FeSiNbBCuCr metallic glass was immune to pitting corrosion in simulated industrial environments, since the current density decreased when the potential scan direction is reversed and it is identified that no pit formed on surface after immersion test. Though no hysteresis loop is observed and E_{corr} shifted toward more anodic values from the cyclic polarization curve, the formation of pits occurs when the anodic branch is enlarged during the forward scan [98]. The size of corrosion pit is less than 50 μm in the PBS solution [99], and the pits are distributed inhomogeneous on the surface of Zr-based metallic glass in NaCl solution [100]. The formation of pits is attributed from the broken of the passive film or irregular microstructure on the surface [101]. Jiang and coworkers [102] found that almost all pits were passed through by shear bands for as-cast sample, while the pit was distributed randomly after annealing.

Gostin et al. [103] considers that no pitting propagation is attributed from the high repassivation ability due to the high content of the beneficial Mo in its composition, although the yttrium oxide particle provides a favorable location for pit formation and local dissolution is initiated at their interface with the glassy matrix. However, Gostin et al. [104] also found that a pitting-like process occurred for the glassy alloy with high concentration of C, as the initial breakdown of passive film caused by the sudden direct exposure of the alloy surface to the electrolyte subsequent to local rupturing of the C-rich layer by growing CO_2 bubbles. Liu and coworkers [105] reported the pitting was initiated since the formation of a nanoscale Cr-depleted zone near the intersplat due to oxidation effect during thermal spraying, as shown in **Figure 12**. Paillier et al. [106] reported that Cu-rich nanocrystals of 5–10 nm were formed inside the corrosion pits during the corrosion process, as shown in **Figure 13**. The corrosion mechanisms of is feasible that elements like Zr, Ti, and Al mainly dissolve in solution whereas Cu and probably Ni is prone to form nanocrystals on the surface covered by a passive oxide layer, as in **Figure 13(a)**, the structure vanishes with the complete removing of the surface oxide by HF (**Figure 13(b)**). On the bare surface alloy without native oxide layer, the small pits develop first with the bow-like morphology, and then, because the corrosion appears to proceed quicker in the vertical direction, and goes along with the canyon-like morphology. Very deep trenches are indeed hollowed leading to a canyon aspect, as shown in **Figure 13(c)**.

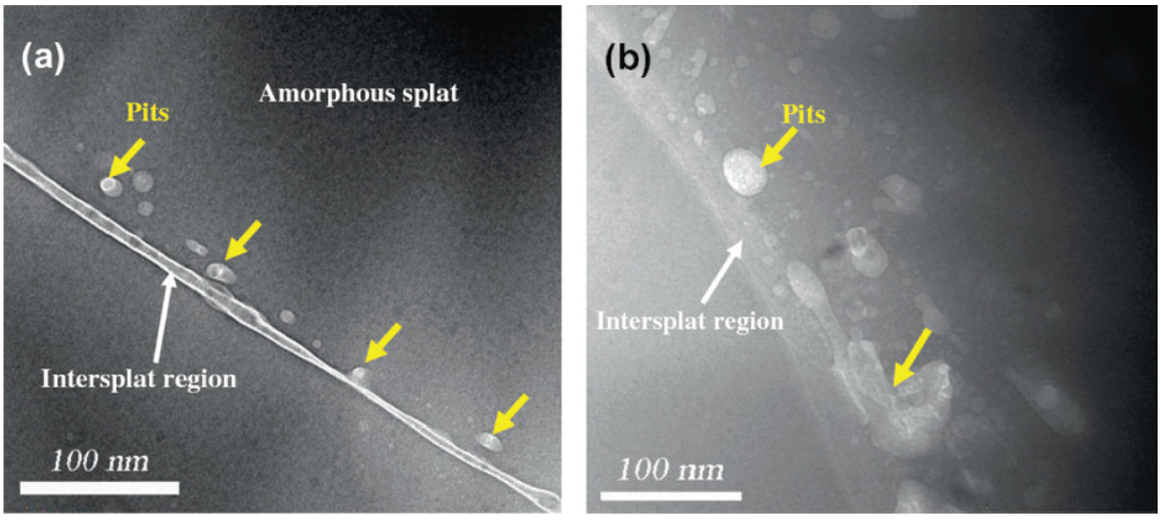

Figure 12. TEM images of the corroded morphologies of the amorphous coating after immersion in 6 M NaCl solution for 1 h (a) and 2 h (b) [105].

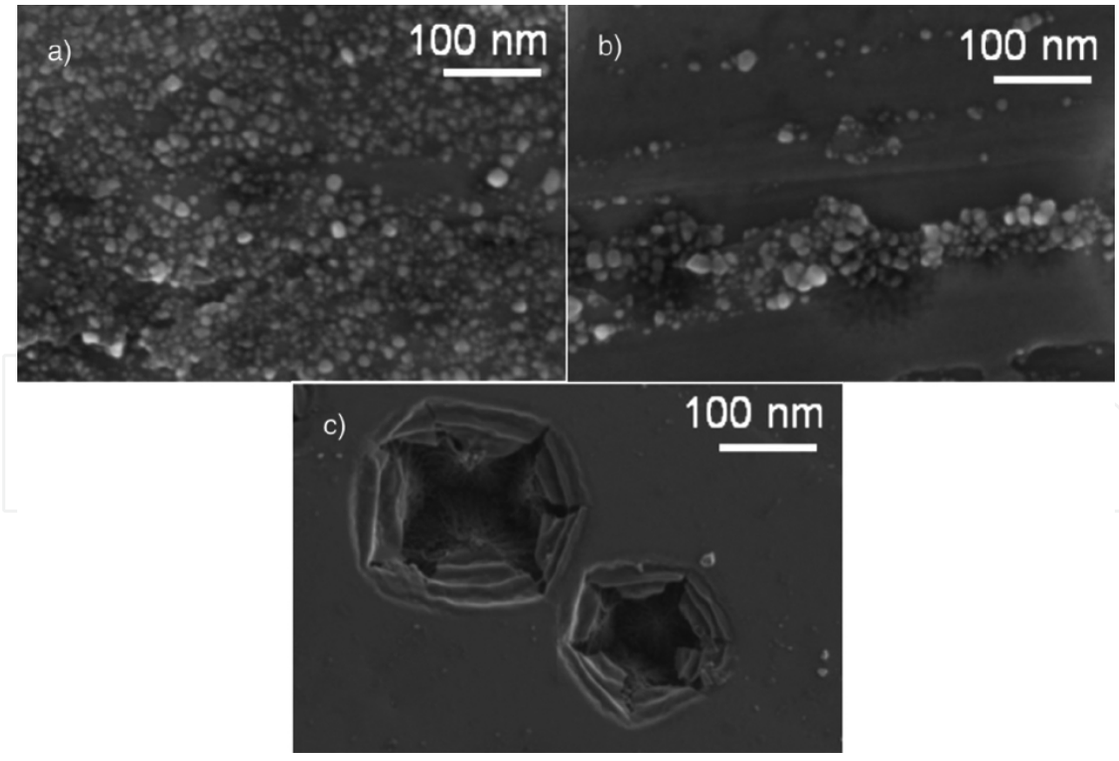

Figure 13. SEM images of $Zr_{59}Ti_3Cu_{20}Al_{10}Ni_8$ after different immersion times in HF 0.1%: (a) 60 s, (b) 120 s, and (c) 180 s [106].

http://dx.doi.org/10.5772/63677

5. Electrocatalytic properties of metallic glasses

Metallic glasses have gained considerable attention in catalysis research due to their unique structural and chemical properties [107], such as the unique atomic structure with a short-range ordering of the constituents, the large flexibility in their chemical composition compared to that of crystalline alloys, the structural and chemical homogeneity, the high reactivity due to their metastable structure, and the excellent conductivity for electricity and heat. Some investigations about the electrocatalytic activity of metallic glasses for the hydrogen evolution reaction or oxygen reduction reaction, such as Co- [108, 109], Zr- [110, 111], Ni- [113], Cu- [114], Pt- [115, 116], and Au-based [117] metallic glasses, are done in last few decades. However, Fe-based metallic glasses are the most attractive as catalytic material. Since the first catalytic materials of Fe-based metallic glass were reported in 1981 [118], a larger number of investigations have be done [118–123], such as the $Fe_{82.7}B_{17.8}$ amorphous ribbon used as a catalyst for the Fischer-Tropsch-type reaction of CO + H_2 [119], amorphous Fe-Zr precursor for ammonia synthesis [120], amorphous FeNiCrPB alloy as catalysts for acetylene hydrogenation [121] and hydrogen evolution [122,123]. The chromium effect on the catalytic activity for FeNiCrPB metallic glass is shown in **Figure 14**. It can be seen that the catalytic activity is strongly affected by Cr presence, while catalytic efficiency is independent of Cr content.

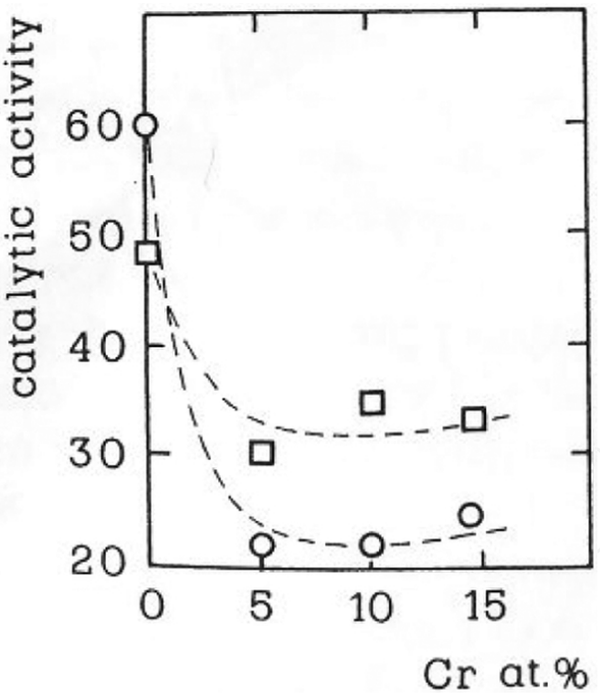

Figure 14. Catalytic activity vs. % Cr: ○, amorphous; □, crystalline [122].

The famous composition of $Fe_{60}Co_{20}Si_{10}B_{10}$ (G14) [124] is firstly reported in 1988, exhibiting good electrocatalytic activity for hydrogen evolution reaction (HER) comparable with Pt. A comparison of kinetics parameters between G14 and pure Fe, vit.7505, pure Pt is illustrated in **Table 6**. With increasing temperature the exchange current densities i_0 of G14 is significant-

ly greater than that of the polycrystalline iron. After this, the relationship between electrocatalytic activity of hydrogen evolution and crystallization [125], anodic treatment [126], and anodic dissolution [127] of amorphous G14 have been investigated in KOH solution. The results indicate amorphous G14 exhibits higher electrocatalytic activities compared with their crystalline alloys. This enhancement is not related to the electronic properties of metallic glass.

Electrode	T (K)	i_0 (A/cm^2)	b (–mV)
Fe (poly)	298	1.0×10^{-5}	135
	323	3.3×10^{-5}	140
	348	4.0×10^{-5}	150
$Fe_{78}Si_{11}B_{11}$	298	1.0×10^{-6}	140
	323	5.0×10^{-5}	150
	348	1.6×10^{-4}	155
$Fe_{60}Co_{20}Si_{10}B_{10}$	298	1.0×10^{-6}	95
	323	4.8×10^{-5}	140
	348	2.7×10^{-4}	150
Pt (poly)	298	2.4×10^{-5}	120
	323	4.8×10^{-5}	150
	348	3.3×10^{-4}	170

Table 6. Electrocatalytic activity parameters of the cathodic hydrogen evolution for G14 and pure Fe, vit. 7505($Fe_{78}Si_{11}B_{11}$), pure Pt.

The electrocatalytic properties are affected not only by the composition of alloy, but also by the surface composition and/or surface area by chemical pretreatment. The catalytic studies [128] on the hydrogenation of carbon monoxide by Fe-based alloy indicated that the activity is augmented by a treatment in HNO_3 solution. Guczi et al. [129] thought that the surface composition and valence state determined in depth were related to the catalytic activity and selectivity revealed in CO + H_2 reaction. An increased number of nickel and iron sites by removing of the prevailing boron oxide, iron oxide, and iron oxide layer after HCl treatment was responsible for the enhanced catalytic activity, as shown in **Figure 15**, that is, the activity of the FeB sample in as-received state was about twice that observed for the FeNiB sample, on the other hand, comparing the HCl etched samples, the activity of the FeNiB alloy was about 30 times higher than that of the FeB ribbon.

The electrocatalytic activity of $Fe_{40}Ni_{40}P_{14}B_6$ metallic glass [130] is improved for HER by acid pretreatment with 1 M HF or HNO_3 for 10 min, since a porous structure with highly roughed and numerous small craters resulted from the selectively leachability of phosphorous from the surface of $Fe_{40}Ni_{40}P_{14}B_6$ metallic glass enhanced the electrode surface area in comparison to the as-polished surface.

http://dx.doi.org/10.5772/63677

The mechanism of hydrogen evolution reaction at the metal electrode in alkaline solution is based on three-step reactions as following:

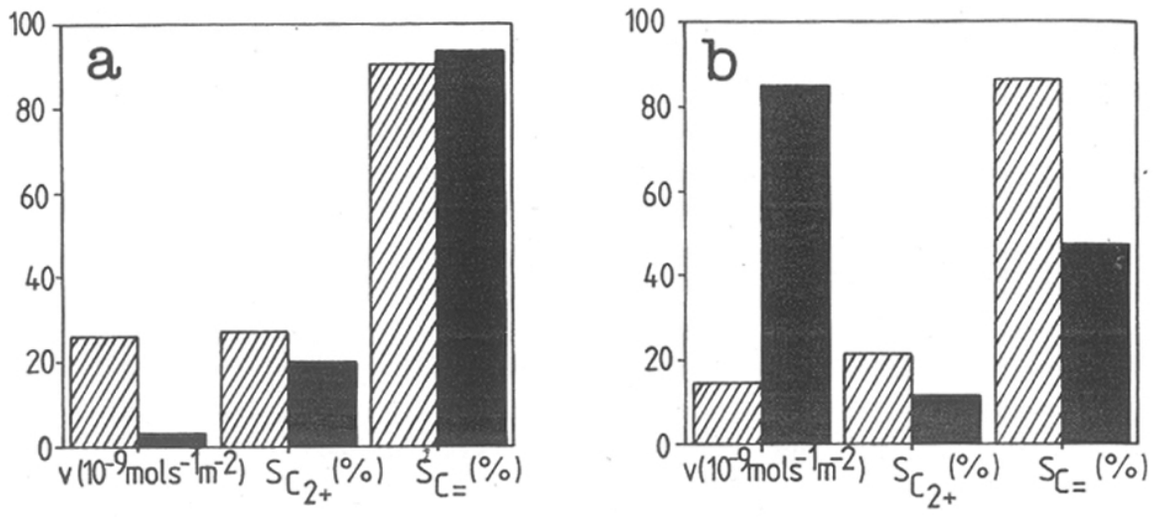

Figure 15. Catalytic activity, S_{c2+} and S_{c-} selectivities over (a) $Fe_{80}B_{20}$, (b) $Fe_{40}Ni_{20}B_{20}$. Hatched: as received. Full black: treated with HCl [129].

Electronation of water with adsorption of hydrogen—Volmer reaction is shown in Eq. (1):

$$M + H_2O + e \Leftrightarrow MH_{ads} + OH^- \quad (1)$$

Electrochemical desorption of H_2—Heyrouvsky reaction is shown in Eq. (2):

$$MH_{ads} + H_2O + e \Leftrightarrow M + H_2 + OH^- \quad (2)$$

Chemical desorption—Tafel reaction is shown in Eq. (3):

$$2MH_{ads} \Leftrightarrow 2M + H_2 \quad (3)$$

Due to involving the transfer of electron from the electrode surface, the density of electrons close to the energy level of metal surface is an important parameter governing electrocatalytic reaction activity. However, it is difficult to estimate during HER, so the efficiency is usually evaluated with overpotential η, Tafel slope b, and exchange current density i_0. The performance of cathodic electrode with respect to HER is primarily characterized by the overpotential which is given by the working electrode potential minus the reversible potential. A linear relationship exists between the overpotential and the cathodic current density as shown in Eq. (4) [131]:

$$\eta = a + b\log(i) \tag{4}$$

where a is constant, b is the Tafel slope, and the exchange current density $i_0 = 10^{-a/b}$. The Tafel slope is mainly affected by the reaction mechanism. In the case of identical Tafel slope, the exchange current density is mainly affected by the effective surface area.

Some Fe-based metallic glasses with high electrocatalytic efficiency are reported, such as a low overpotential η_{300} = 318 mV for amorphous $Fe_{71}Mo_{29}$ alloy [132] at 30% KOH solution at 303 K, a low Tafel slope b = 95 mV and a large exchange current density i_0 = 1 μm/cm^2 for amorphous $Fe_{60}Co_{20}Si_{10}B_{10}$ alloy [124] at 1 M KOH solution at 298 K, and $Fe_{59.5}C_3Si_{7.3}B_{8.5}P_{5.7}Mo_{2.5}Co_{13.5}$ alloy with b =110 mV and i_0 = 16 μm/cm^2 [133]. It is evident that the Tafel slope as well as overpotential decrease with increase of Mo content at the same conditions [132]. However, the Tafel slope does not change with replace of Co for Fe in the amorphous FeCoB alloy [134]. The results of Tafel slope are considered that the effective transfer coefficients for the dissolution of boron and the metals are equal.

6. Summary

The investigation of corrosion resistance of metallic glass is attractive for allover researchers in materials science and engineering, since the unique structure and properties, extensive potential application. Most researches are focus on the effects of element addition and nanocrystallization on the general and local corrosion resistance in various environments. Certain elements are identified are quite effective in improving the corrosion resistance. And the crystallization of metallic glass is usually deleterious for the corrosion resistance. In general, the decreasing is the corrosion resistance of metallic glasses, the increasing is the solution aggressiveness, especial for the chloride ion concentration. Unfortunately, the mechanism of pitting corrosion of metallic glass is not clear, as that of conventional materials such as stainless steel. As practical application of the metallic glasses in industrial field, some metallic glasses such as Fe-based metallic glass are used as anticorrosion or antiwearing materials. The coating is one of effective methods. During the coating processing, some inclusion, oxidation, crystallization, and even second particle as reinforcement phase in the coat layer is inevitable. However, the effect of these particles on the general and pitting corrosion resistance is seldom reported. Therefore, further investigation about the pitting corrosion is necessary to the industrial application of metallic glass.

Acknowledgements

The work was supported by the National Natural Science Foundation of China (51461031) and the Department of Education Fund of Jiangxi (GJJ150733). Thanks for their understanding and support of my wife, Yanmei Zhang, and my son, Bob.

Author details

Shanlin Wang

Address all correspondence to: slwang70518@nchu.edu.cn

National Defense Key Discipline Laboratory of Light Alloy Processing Science and Technology, Nanchang hangkong university, Nanchang, China

References

[1] Naka M, Hashinoto K, Masumoto T. Effect of metalloidal elements on corrosion resistance of amorphous iron-chromium alloys. J. Non-Cryst. Solids. 1978; 28: 403–413.

[2] Liaw MMP. Bulk metallic glasses an overview. Springer. USA, 2008, p. 10.

[3] Scully J R, Gebert A, Payer J H. Corrosion and related mechanical properties of bulk metallic glasses. J. Mater. Res. 2007; 17(6): 302–313.

[4] Peter W H, Buchanan R A, Liu C T. Localized corrosion behavior of a zirconium-based bulk metallic glass relative to its crystalline state. Intermetallics. 2002; 10: 1157–1162.

[5] Klement W, Willens R H, Duwez P. Non-crystalline structure in solidified gold-silicon alloys. Nature. 1960; 187: 869–870.

[6] Li Y H, Zhang W, Inoue A. Effects of Ni addition on the glass-forming ability, mechanical properties and corrosion resistance of Zr–Cu–Al bulk metallic glasses. Mater. Sci. Eng. A. 2011; 528: 8551–8556.

[7] Li Y H, Zhang W, Inoue A. Glass-forming ability and corrosion resistance of Zr-based Zr–Ni–Al bulk metallic glasses. J. Alloys Compd. 2012; 536s: S117–S121.

[8] Kawashima A, Ohmura K, Inoue A. The corrosion behavior of Zr-based bulk metallic glasses in 0.5 M NaCl solution. Corr. Sci. 2011; 53: 2778–2784.

[9] Huang H H, Huang H M, Lin M C. Enhancing the bio-corrosion resistance of Ni-free ZrCuFeAl bulk metallic glass through nitrogen plasma immersion ion implantation. J. Alloys Compd. 2014; 615: s660–s665.

[10] Zhao G H, Aune R E, Mao H H. Degradation of Zr-based bulk metallic glasses used in load-bearing implants: a tribocorrosion appraisal. J. Mech. Behav. Biol. Mater. 2016; 60: 56–67.

[11] Hua N B, Huang L, Zhang T. Corrosion behavior and in vitro biocompatibility of Zr–Al–Co–Ag bulk metallic glasses: an experimental case study. 2012; 358: 1599–1640.

[12] Hua N B, Zhang T. Glass-forming ability, crystallization kinetics, mechanical property, and corrosion behavior of Zr–Al–Ni–Ag glassy alloys. J. Alloys Compd. 2014; 602: 339–345.

[13] Zhang C, Li N, Liu L. Enhancement of glass-forming ability and bio-corrosion resistance of Zr–Co–Al bulk metallic glasses by the addition of Ag. J. Alloys Compd. 2010; 504: s163–s167.

[14] Guan B R, Shi X T, Qin F X. Corrosion behavior, mechanical properties and cell cytotoxity of Zr-based bulk metallic glasses. Intermetallics. 2016; 72: 69–75.

[15] Nie X P, Xu X M, Jiang J Z. Effect of microalloying of Nb on corrosion resistance and thermal stability of ZrCu-based bulk metallic glasses. J. Non-Cryst. Solids. 2009; 355: 203–207.

[16] Li Y H, Zhang W, Qin F X. Mechanical properties and corrosion resistance of a new $Zr_{56}Ni_{20}Al_{15}Nb_4Cu_5$ bulk metallic glass with a diameter up to 25 mm. J. Alloys Compd. 2014; 615: s71–s74.

[17] Zhuang Y X, Wang S C, Wang C J. Effect of Ti on microstructure, mechanical and corrosion properties of $(Zr_{0.55}Al_{0.1}Ni_{0.05}Cu_{0.3})_{100-x}Ti_x$ bulk metallic glasses. Trans. Nonferrous Met. Soc. China. 2016; 26: 138–143.

[18] Liu Z Q, Huang L, Zhang T. Novel low Cu content and Ni-free Zr-based bulk metallic glasses for biomedical applications. J. Non-Cryst. Solids. 2013; 363: 1–5.

[19] Asami K, Qin C L, Zhang T. Effect of additional elements on the corrosion behavior of a Cu–Zr–Ti bulk metallic glass. Mater. Sci. Eng. A. 2004; 375: 235–239.

[20] Liu B, Liu L. Determination of isothermal section of Fe-Ni-Zr ternary system at 1198 K. Acta Metall. Sin. 2007; 20(6): 398–402.

[21] Qin C L, Asami K, Zhang T. The corrosion behavior of Zr-based bulk metallic glasses in 0.5 M NaCl solution. Mater. Trans. 2003; 44: 1042–1147.

[22] Pi J H, Pan Y, Wu J L. Influence of Minor Addition of In on corrosion resistance of Cu-based bulk metallic glasses in 3.5% NaCl solution. Rare Met. Mater. Eng. 2014; 43: 32–35.

[23] Chen S F, Lin S L, Chen J K. Thermal stability and corrosion behavior of Cu–Zr–Al–Y bulk metallic glass. Intermetallics. 2010; 18: 1954–1957.

[24] Zhang C Z, Wang J H, Qiu N N. Facile and large-scale syntheses of nanocrystal rare earth metal–organic frameworks at room temperature and their photoluminescence properties. J. Rare Earth. 2015; 33: 680–685.

[25] Zhang C Z, Qiu N N, Kong L L. Thermodynamic and structural basis for electrochemical response of Cu–Zr based metallic glass. J. Alloys Compd. 2015; 645: 487–490.

[26] Pang S J, Liu Y, Zhang T. New Ti-based Ti–Cu–Zr–Fe–Sn–Si–Ag bulk metallic glass for biomedical applications. J. Alloys Compd. 2015; 625: 323–327.

[27] Guo Y, Bataev I, Georgarakis K. Ni- and Cu-free Ti-based metallic glasses with potential biomedical application. Intermetallics. 2015; 63: 86–96.

[28] Fornell J, Pellicer E, Sort J. Improved plasticity and corrosion behavior in Ti–Zr–Cu–Pd metallic glass with minor additions of Nb: an alloy composition intended for biomedical applications. Mater. Sci. Eng. A. 2013; 559: 159–164.

[29] Liu N, Wu P H, Zhou P J. Rapid solidification and liquid-phase separation of undercooled CoCrCuFeNi high-entropy alloys. Intermetallics. 2016; 72: 44–52.

[30] Wang J F, Huang S, Li Y. Microstructure, mechanical and bio-corrosion properties of Mn-doped Mg–Zn–Ca bulk metallic glass composites. Mater. Sci. Eng. C. 2013; 33: 3832–3833.

[31] Gu X N, Zheng Y F, Zhong S P. Corrosion of, and cellular responses to Mg–Zn–Ca bulk metallic glasses. Biomaterials. 2010; 31: 1093–1103.

[32] Zhang X L, Chen G. The effects of microalloying on thermal stability, mechanical property and corrosion resistance of Mg-based bulk metallic glasses. J. Non-Cryst. Solids. 2012; 358: 1319–1323.

[33] Wang R R, Wang Y Y, Yang J. Influence of heat treatment on the mechanical properties, corrosion behavior, and biocompatibility of $Zr_{56}Al_{16}Co_{28}$ bulk metallic glass. J. Non-Cryst. Solids. 2015; 411: 45–52.

[34] Guo S F, Liu Z, Chan K C. A plastic Ni-free Zr-based bulk metallic glass with high specific strength and good corrosion properties in simulated body fluid. Mater. Lett. 2012; 84: 81–84.

[35] Fornell J, Steenberge N V, Varea A. Enhanced mechanical properties and in vitro corrosion behavior of amorphous and devitrified $Ti_{40}Zr_{10}Cu_{38}Pd_{12}$metallic glass. J. Mech. Behav. Biol. Mater. 2011; 4: 1709–1717.

[36] Huang C H, Lai J J, Wei T Y. Improvement of bio-corrosion resistance for $Ti_{42}Zr_{40}Si_{15}Ta_3$ metallic glasses in simulated body fluid by annealing within supercooled liquid region. Mater. Sci. Eng. C. 2015; 52: 144–150.

[37] Gonzalez S, Pellicer E, Surinach S. Mechanical and corrosion behaviour of as-cast and annealed $Zr_{60}Cu_{20}Al_{10}Fe_5Ti_5$ bulk metallic glass. Intermetallics. 2012; 28: 149–155.

[38] Wang D P, Wang S L, Wang J Q. Relationship between amorphous structure and corrosion behaviour in a Zr–Ni metallic glass. Corr. Sci. 2012; 59: 88–95.

[39] Gu Y, Zheng Z, Niu S Z. The seawater corrosion resistance and mechanical properties of $Cu_{47.5}Zr_{47.5}Al_5$ bulk metallic glass and its composites. J. Non-Cryst. Solids. 2013; 380: 135–140.

[40] Wang J F, Huang S, Wei Y Y. Enhanced mechanical properties and corrosion resistance of a Mg–Zn–Ca bulk metallic glass composite by Fe particle addition. Mater. Lett. 2013; 91: 311–314.

[41] Zhang X L, Chen G, Bauer T. Mg-based bulk metallic glass composite with high bio-corrosion resistance and excellent mechanical properties. Intermetallics. 2012; 29: 56–60.

[42] Kai W, Kao P C, Chen W S . The oxidation behavior of a $Ti_{50}Cu_{28}Ni_{15}Sn_7$ bulk metallic glass at 400–500 °C. J. Alloys Compd. 2010; 504s: s180–s185.

[43] Subramanian B. In vitro corrosion and biocompatibility screening of sputtered $Ti_{40}Cu_{36}Pd_{14}Zr_{10}$ thin film metallic glasses on steels. Mater. Sci. Eng. C. 2014; 47: 48–56.

[44] Xie G Q, Qin F X, Zhou S L. Corrosion behaviour of porous Ni-free Ti-based bulk metallic glass produced by spark plasma sintering in Hanks' solution. Intermetallics. 2014; 44: 55–59.

[45] Gebert A, Gostin P F, Schultz L. Effect of surface finishing of a Zr-based bulk metallic glass on its corrosion behaviour. Corr. Sci. 2010; 52: 1711–1720.

[46] Gebert A, Consustell A, Greer A L. Effect of shot-peening on the corrosion resistance of a Zr-based bulk metallic glass. Scripta Mater. 2010; 62: 635–638.

[47] Gebert A, Gostin P F, Uhlemann M. Interactions between mechanically generated defects and corrosion phenomena of Zr-based bulk metallic glasses. Acta Mater. 2012; 60: 2300–2309.

[48] An W K, Cai A H, Xiong X. Effect of tension on corrosive and thermal properties of $Cu_{60}Zr_{30}Ti_{10}$ metallic glass. J. Alloys Compd. 2013; 563: 55–62.

[49] Pourgashti M H, Marzbanrad E, Ahnadi E. Corrosion behavior of $Zr_{41.2}Ti_{13.8}Ni_{10}Cu_{12.5}Be_{22.5}$ bulk metallic glass in various aqueous solutions. Mater. Des. 2010; 31: 2676–2679.

[50] Gebert A, Buchholz K, Eckert J. Hot water corrosion behaviour of Zr–Cu–Al–Ni bulk metallic glass. Mater. Sci. Eng. A. 2001; 316: 60–65.

[51] Ningshen S, Kamachi Mudali U, Krishnan R. Corrosion behavior of Zr-based metallic glass coating on type 304L stainless steel by pulsed laser deposition method. Surf. Coat. Technol. 2011; 205: 3961–3966.

[52] Cai A H, Xiong X, Liu Y. Corrosion behavior of $Cu_{55}Zr_{35}Ti_{10}$ metallic glass in the chloride media. Mater. Chem. Phys. 2012; 134: 938–944.

[53] Wang T, Wu Y D, Hui X D. Novel Ti-based bulk metallic glasses with superior plastic yielding strength and corrosion resistance. Mater. Sci. Eng. A. 2015; 642: 297–303.

[54] Guo S F, Chan K C, Jiang X Q. Atmospheric RE-free Mg-based bulk metallic glass with high bio-corrosion resistance. J. Non-Cryst. Solids. 2013; 379: 107–111.

[55] Gebert A, Mummert K, Eckert J. Electrochemical investigations on the bulk glass forming $Zr_{55}Cu_{30}Al_{10}Ni_5$ alloy. Mater. Corros. 1997; 48: 293–297.

[56] Vincent S, Khan A F, Bhatt J. Corrosion characterization on melt spun $Cu_{60}Zr_{20}Ti_{20}$ metallic glass: An experimental case study. J. Non-Cryst. Solids. 2013; 379: 48–53.

[57] Long Z L, Shao Y, Inoue A. Cr effects on magnetic and corrosion properties of Fe–Co–Si–B–Nb–Cr bulk glassy alloys with high glass-forming ability. Intermetallics. 2007; 15: 1453–1458.

[58] Pardo A, Otero E, Merino M C. The influence of Cr addition on the corrosion resistance of $Fe_{73.5}Si_{13.5}B_9Nb_3Cu_1$ metallic glass in marine environments. Corr. Sci. 2002; 44: 1193–1211.

[59] Pardo A, Merino M C, Otero E. Influence of Cr additions on corrosion resistance of Fe- and Co-based metallic glasses and nanocrystals in H_2SO_4. J. Non-Cryst. Solids. 2006; 352: 3179–3190.

[60] Wang S L, Yi S. The corrosion behaviors of Fe-based bulk metallic glasses in a sulfuric solution at 70 °C. Intermetallics. 2010; 18: 1950–1953.

[61] Wang Z M, Ma Y T, Wang J Q. Influence of yttrium as a minority alloying element on the corrosion behavior in Fe-based bulk metallic glasses. Electrochem. Acta. 2008; 54: 261–269.

[62] Long Z L, Chang C T, Inoue A. Corrosion behavior of Fe-based ferromagnetic (Fe, Ni)–B–Si–Nb bulk glassy alloys in aqueous electrolytes. J. Non-Cryst. Solids. 2008; 354: 4609–4613.

[63] Souza C A C, Mar J E, Kiminami C S. Influence of composition and partial crystallization on corrosion resistance of amorphous Fe–M–B–Cu (M = Zr, Nb, Mo) alloys. J. Non-Cryst. Solids. 2001; 284: 99–104.

[64] Zohdi H, Shahverdi H R, Hadavi S M M. Effect of Nb addition on corrosion behavior of Fe-based metallic glasses in Ringer's solution for biomedical applications. Electrochem. Commun. 2011; 13: 840–843.

[65] Kiminami C S, Souza C A C, Botta W J. Partial crystallization and corrosion resistance of amorphous Fe-Cr-M-B (M = Mo, Nb) alloys. J. Non-Cryst. Solids. 2010; 356: 2651–2657.

[66] Wang S L, Li H X, Yi S. Effects of Cr contents in Fe-based bulk metallic glasses on the glass forming ability and the corrosion resistance. Mater. Chem. Phys. 2009; 13: 878–883.

[67] Lopez M F, Escudero M L, Vida E. Corrosion behaviour of amorphous FeCrNi(Si,P) alloys. Electrochem. Acta. 1997; 42: 659–665.

[68] Pang S J, Zhang T, Inoue A. Bulk glassy Fe–Cr–Mo–C–B alloys with high corrosion resistance. Corros. Sci. 2002; 44: 1847–1856.

[69] Ha H M, Miller J R, Payer J H. Devitrification of Fe-based amorphous metal SAM 1651 and the effect of heat-treatment on corrosion behavior. Eletrochem. J. Soc. 2009; 156: 246–252.

[70] Baron A, Szewieczek D, Nawrat G. Corrosion of amorphous and nanocrystalline Fe-based alloys and its influence on their magnetic behavior. Electrochem. Acta. 2007; 52: 5690–5695.

[71] Souza C A C, May J E, Kiminami C S. Corrosion resistance of amorphous and nanocrystalline Fe–M–B (M Zr, Nb) alloys. J. Non-Cryst. Solids. 2000; 273: 282–288.

[72] Long Z L, Shen B L, Inoue A. Cr effects on magnetic and corrosion properties of Fe–Co–Si–B–N. Intermetallics. 2007; 15: 1453–1458.

[73] Marzo F F, Pierma A R, Vega M M. Effect of irreversible structural relaxation on the electrochemical behavior of $Fe_{78-x}Si_{13}B_9Cr$ (x = 3, 4, 7) amorphous alloys. J. Non-Cryst. Solids. 2003; 329: 108–114.

[74] Souza C A C, Kuri S E, Politti F S. Corrosion resistance of amorphous and polycrystalline FeCuNbSiB alloys in sulphuric acid solution. J. Non-Cryst. Solids. 1999; 247: 69–73.

[75] Liu G, An Y L, Chen J M. Structure and corrosion behavior of iron-based metallic glass coatings prepared by LPPS. Appl. Surf. Sci. 2012; 258: 5380–5386.

[76] Zhou Z, Wang L, Wang F C. Formation and corrosion behavior of Fe-based amorphous metallic coatings by HVOF thermal spraying. Surf. Coat. Technol. 2009; 204: 563–570.

[77] Zhang S D, Zhang W L, Wang J Q. Characterisation of three-dimensional porosity in an Fe-based amorphous coating and its correlation with corrosion behaviour. Corr. Sci. 2015; 93: 211–221.

[78] Wang S L, Cheng J C, Yi S. Corrosion resistance of Fe-based amorphous metallic matrix coating fabricated by HVOF thermal spraying. Trans. Nonferrous Met. Soc. China. 2014; 24: 146–151.

[79] Cui C, Hou W. Properties of Fe-based amorphous alloy coatings with Al_2O_3–13% TiO_2 deposited by plasma spraying. Rare Met. Mater. Eng. 2014; 43: 2576–2579.

[80] Yasir M, Zhang C, Liu L. Wear behaviors of Fe-based amorphous composite coatings reinforced by Al_2O_3 particles in air and in NaCl solution. Mater. Des. 2015; 88: 207–213.

[81] Yugeswarn S, Kobayashi A. Characterization of gas tunnel type plasma sprayed TiN reinforced Fe-based metallic glass coatings. J. Alloys Compd. 2013; 551: 168–175.

[82] Zhou H, Zhang C, Wang W. Microstructure and mechanical properties of Fe-based amorphous composite coatings reinforced by stainless steel powders. J. Mater. Sci. Technol. 2014; 31: 43–47.

[83] Zhu Y Y, Li Z G, Li R F. Microstructure and property of Fe–Co–B–Si–C–Nb amorphous composite coating fabricated by laser cladding process. Appl. Surf. Sci. 2013; 280: 50–54.

[84] Pang S J, Zhang T, Inoue A. Synthesis of Fe–Cr–Mo–C–B–P bulk metallic glasses with high corrosion resistance. Acta Mater. 2002; 50: 489–497.

[85] Wang Y, Jiang S L, Wang J Q. Electrochemical behaviour of Fe-based metallic glasses in acidic and neutral solutions. Corr. Sci. 2012; 63: 159–173.

[86] Qiao D C, Green B, Morrison M. Bulk metallic glass. Rev. Adv. Mater. Sci. 2008; 18: 149–153.

[87] Czachor M J. Effect of nitrogen and sensitization on the microstructure and pitting corrosion behavior of AISI Type 316LN stainless steels. ISIJ Int. 1991; 31: 1170–1178.

[88] Patsalas P, Lekatou A, Pavlidou E. Surface properties and activity of Fe–Ni–B ternary glasses. J. Alloys Compd. 2007; 434: 229–233.

[89] Li H X, Yi S. Corrosion behaviors of bulk metallic glasses $Fe_{66.7}C_{7.0}Si_{3.3}B_{5.5}P_{8.7}Cr_{2.3}Al_{2.0}Mo_{4.5}$ having different crystal volume fractions. Mater. Chem. Phys. 2008; 112: 305–309.

[90] Wang Y B, Li H F, Zheng Y F. Corrosion performances of a nickel-free Fe-based bulk metallic glass in simulated body fluids. Electrochem. Commun. 2009; 11: 2187–2190.

[91] Zhou Z, Wang L, He D Y. Effect of feed stock particle sizes on wear resistance of plasma sprayed Fe-based amorphous coatings. Surf. Coat. Technol. 2011; 20: 495–502.

[92] Wang L, Chao Y S. Corrosion behavior of $Fe_{41}Co_7Cr_{15}Mo_{14}C_{15}B_6Y_2$ bulk metallic glass in NaCl solution. Mater. Lett. 2012; 69: 76–78 .

[93] Guo S F, Chan K C, Xie S H. Novel centimeter-sized Fe-based bulk metallic glass with high corrosion resistance in simulated acid rain and seawater. J. Non-Cryst. Solids. 2013; 369: 29–33.

[94] Botta W J, Berger J E, Kiminami C S. Corrosion resistance of Fe-based amorphous alloys. J. Alloys Compd. 2014; 586: s105–s110.

[95] Lekatou A, Marinou A, Patsalas P. Aqueous corrosion behaviour of Fe–Ni–B metal glasses. J. Alloys Compd.. 2009; 48: 514–518.

[96] Poon S J, Shiflet G. J, Guo F Q. Glass formability of ferrous- and aluminum-based structural metallic alloys. J. Non-Cryst. Solids. 2003; 317: 1–9.

[97] Shan X, Ha H, Payer J H. Comparison of crevice corrosion of Fe-based amorphous metal and crystalline Ni-Cr-Mo alloy. Metall. Mater. Trans. A. 2009; 40: 1324–1333.

[98] Fornell J, Gonzalez S, Sort J. Deformation and fracture behavior of corrosion-resistant, potentially biocompatible $Ti_{40}Zr_{10}Cu_{38}Pd_{12}$ bulk metallic glass. J. Alloys Compd. 2012; 536: s74–s77.

[99] Hua N B, Zheng Z Q, Fang H. Dry and lubricated tribological behavior of a Ni- and Cu-free Zr-based bulk metallic glass. J. Non-Cryst. Solids. 2015; 426: 63–71.

[100] Kou H C, Li Y, Zhang T. Electrochemical corrosion properties of Zr- and Ti-based bulk metallic glasses. Trans. Nonferrous Met. Soc. China. 2011; 21: 552–557.

[101] Green B A, Steward R V, Kim I. In situ observation of pitting corrosion of the $Zr_{50}Cu_{40}Al_{10}$ bulk metallic glass. Intermetallics. 2009; 17: 568–571.

[102] Nie X P, Cao Q P, Jiang J Z. The pitting corrosion behavior of shear bands in a Zr-based bulk metallic glass. Scripta Mater. 2012; 67: 376–379.

[103] Gosin P F, Gebert A, Schultz L. Comparison of the corrosion of bulk amorphous steel with conventional steel. Corr. Sci. 2010; 52: 273–281.

[104] Gostin P F, Oswald S, Gebert A. Acid corrosion process of Fe-based bulk metallic glass. Corr. Sci. 2012; 62: 112–121.

[105] Zhang C, Chan K C, Liu L. Pitting initiation in Fe-based amorphous coatings. Acta. Mater. 2012; 60: 4152–4159.

[106] Paillier J, Mickel C, Flaviu P. Characterization of corrosion phenomena of Zr–Ti–Cu–Al–Ni metallic glass by SEM and TEM. Mater. Charact. 2010; 61: 1000–1008.

[107] Ertl G, Knozinger H, Weitkamp J. Preparation of solid catalysts. Springer, USA. 1999; p. 43.

[108] Carim A I, Saadi F H, Levis N S. Stabilization of *n*-cadmium telluride photoanodes for water oxidation to O_2(g) in aqueous alkaline electrolytes using amorphous TiO_2 films formed by atomic-layer deposition. J. Mater. Chem. A. 2014; 2: 138–35.

[109] Jukic A, Piljac J, Hukovic M M. Electrocatalytic behavior of the $Co_{33}Zr_{67}$ metallic glass for hydrogen evolution. A: Chemical, 2001, 166: 293–302.

[110] Hukovic M M, Jukic A. Correlation of electronic structure and catalytic activity of Zr–Ni amorphous alloys for the hydrogen evolution reaction. Electrochim. Acta. 2000; 45: 4159–4170.

[111] Mihailov L, Spassov T, Bojinov M. Effect of microstructure on the electrocatalytic activity for hydrogen evolution of amorphous and nanocrystalline Zr–Ni alloys. Inter. J. Hydrogen Energy. 2012; 37: 10499–10506.

[112] Ramos-sanchez G, Pierna A R, Solorza-Feria O. Amorphous $Ni_{59}Nb_{40}Pt_xM_{1-x}$ (M = Ru, Sn) electrocatalysts for oxygen reduction reaction. J. Non-Cryst. Solids. 2008; 354: 5165–5168.

[113] Jiang J H, Zhai R S, Bao X H. Electrocatalytic properties of Cu–Zr amorphous alloy towards the electrochemical hydrogenation of nitrobenzene. J. Alloys Compd. 2003; 354: 248–258.

[114] Sun S G, Lipkowski J. Altounian Z. Electrocatalytic oxidation of formic acid and methanal at the amorphous $Pt_{66}Sb_{34}$ Electrode. J. Electrochem. Soc. 1990; 137: 2443–2451.

[115] Dan Z H, Qin F X, Wada T. Nanoporous palladium fabricated from an amorphous $Pd_{42.5}Cu_{30}Ni_{7.5}P_{20}$ precursor and its ethanol electro-oxidation performance. Electrochim. Acta. 2013; 108: 512–519.

[116] Brunelli K, Dabala M, Frattini R. Structural characterization and electrocatalytic properties of $Au_{30}Zr_{70}$ amorphous alloy obtained by rapid quenching. J. Appl. Electrochem. 2003; 33: 995–1000.

[117] Yokoyama A, Komiyama H, Inoue H. The hydrogenation of carbon monoxide by amorphous ribbons. J. Catal. 1981; 68: 355–361.

[118] Kisfaludi G, Kazar K, Schay Z. Surface characterization and catalytic CO + H_2 reaction on $Fe_{82.2}B_{17.8}$ amorphous alloy. Appl. Surf. Sci. 1985; 24: 225–238.

[119] Baiker A, Schlogl R, Armbruster E. New catalytic materials from amorphous metal alloys. J. Catal. 1989; 107: 329–383.

[120] Carturan G, Cocco G. Amorphous and crystalline FeNiCrPB alloys as catalysts for acetylene hydrogenation. J. Catal. 1984; 90: 178–181.

[121] Kovocs P, Ando T, Ishiwatari M. Electrochemical studies on the potentiostatic hydrogenatiaon of amorphous $Fe_{90}Zr_{10}$ and $Fe_{91}Hf_9$ alloys. J. Electrochem, Soc. 1989; 136: 1958–1961.

[122] Paseka I, Velika J. Hydrogen evolution and hydrogen sorption on amorphous smooth MeP(x) (MeNi, Co and FeNi) electrodes. Electrochem. Acta. 1997; 42: 237–242.

[123] Alemu H, Juttner K. Characterization of the electrocatalytic properties of amorphous metals for oxygen and hydrogen evolution by impedance measurements. Electrochem. Acta. 1988; 33: 1101–1109.

[124] Trudeau M L, Huot J Y, Schulz R. The crystallization of amorphous $Fe_{60}Co_{20}Si_{10}B_{10}$ and its effect on the electrocatalytic activity for H_2 evolution. J. Appl. Phys. 1990; 67: 2333–2342.

[125] Crousier J, Crousier J P, Bellucci F. Electrochemical and electrocatalytic behaviour of iron-base amorphous alloys in 1 M KOH at 25°C. Electrochem. Acta. 1993; 38: 821–825.

[126] Crousier J, Crousier J P, Bellucci F. Anodic dissolution and electrocatalytic properties of $Fe_{60}Co_{20}Si_{10}B_{10}$ amorphous alloy in 1 M KOH. Corros. Sci. 1994; 36: 995–1055.

[127] Albertos F, Harji B H, Kenney C N. Catalytic behaviour of some glassy alloys to the Fischer-Tropsch reaction at high pressures. Appl. Catal. 1990; 65: 85–100.

[128] Guczi L, Kisfaludi G, Schay Z. Surface structure and catalytic activity of rapidly quenched amorphous iron based alloys. III. Effect of surface composition. Appl. Surf. Sci. 1989; 35: 469–480.

[129] Brookes H C, Carruthers C M. The electrochemical and electrocatalytic behaviour of glassy metals. J. Appl. Electrochem. 2005, 35: 903–913.

[130] Trudeau M L, Huot J Y, Schulz R. Nanocrystalline Fe-(Co,Ni)-Si-B: The mechanical crystallization of amorphous alloys and the effects on electrocatalytic reactions. Phys. Rev. B. 1992; 45: 4626–4636.

[131] Niu Z J, Wu T H, Yang F Z. Electrocatalytic activity of electrodeposited amorphous Fe-Mo alloy for hydrogen evolution reaction in alkaline solution. Mater. Protection. 2003; 36: 9–12.

[132] Wang S L, Kim D H, Yi S. Electrocatalytic properties of Fe-based bulk metallic glasses for hydrogen evolution reaction. Korean J. Chem. Eng. 2011; 28: 1672–1676.

[133] Heusler K E, Huerta D. Kinetics and mechanisms of the anodic dissolution of metallic glasses. J. Electrochem. Soc. 1988; 136: 65–71.